MITSUBISHI ELECTRIC RESEARCH LABORATORIES
http://www.merl.com

Reconfigurable Model Predictive Control for Multi-Evaporator Vapor Compression Systems

Burns, D.J.; Danielson, C.; Zhou, J.; Di Cairano, S.

TR2017-083 June 2017

Abstract

This paper considers the control of a multievaporator vapor compression system (ME-VCS) where individual evaporators are permitted to turn on or off. We present a model predictive controller (MPC) that can be easily reconfigured for different on/off configurations of the system. In this approach, only the cost function of the constrained finitetime optimal control problem is updated depending on the system configuration. Exploiting the structure of the system dynamics, the cost function is modified by zeroing elements of the state, input, and terminal cost matrices. The advantage of this approach is that cost matrices for each configuration of the ME-VCS do not need to be stored or computed online. This reduces the effort required to tune and calibrate the controller and the amount of memory required to store the controller parameters in a microprocessor. The reconfigurable MPC is compared with a conventional approach in which individual model predictive controllers are independently designed for each on/off configuration. Simulations show that the reconfigurable MPC method provides similar closed-loop performance in terms of reference tracking and constraint satisfaction to the set of individual model predictive controllers. Further, we show that our controller requires substantially less memory than the alternative approaches. Experiments on a residential two-zone vapor compression system further validate the reconfigurable MPC method.

IEEE Transactions on Control Systems Technology

Reconfigurable Model Predictive Control for Multi-Evaporator Vapor Compression Systems

Daniel J. Burns†, Claus Danielson†, Junqiang Zhou†, and Stefano Di Cairano

***Abstract*—This paper considers the control of a multi-evaporator vapor compression system (ME-VCS) where individual evaporators are permitted to turn on or off. We present a model predictive controller (MPC) that can be easily reconfigured for different on/off configurations of the system. In this approach, only the cost function of the constrained finite-time optimal control problem is updated depending on the system configuration. Exploiting the structure of the system dynamics, the cost function is modified by zeroing elements of the state, input, and terminal cost matrices. The advantage of this approach is that cost matrices for each configuration of the ME-VCS do not need to be stored or computed online. This reduces the effort required to tune and calibrate the controller and the amount of memory required to store the controller parameters in a microprocessor. The reconfigurable MPC is compared with a conventional approach in which individual model predictive controllers are independently designed for each on/off configuration. Simulations show that the reconfigurable MPC method provides similar closed-loop performance in terms of reference tracking and constraint satisfaction to the set of individual model predictive controllers. Further, we show that our controller requires substantially less memory than the alternative approaches. Experiments on a residential two-zone vapor compression system further validate the reconfigurable MPC method.**

***Index Terms*—Vapor Compression Systems, Model Predictive Control, Plug-and-Play Control, Reconfigurable Control.**

I. Introduction

Vapor compression systems (VCS), such as heat pump, refrigeration, and air-conditioning systems, are widely used in industrial and residential applications. The introduction of variable speed compressors, electronically-positioned valves, and variable speed fans to the vapor compression cycle has greatly improved the flexibility of the operation of such systems [1]. This increased actuator flexibility, along with increasing onboard computing power, enables more sophisticated control schemes than traditional on-off logic, or decentralized PI controllers. Model Predictive Control (MPC) offers a flexible and rigorous design process for vapor compression systems in which the constraints are enforced during transients and can be modified as the design evolves. Furthermore, by appropriate design, the resulting controller provides guarantees on feasibility, optimality, convergence, transient performance and stability [2]–[4].

D. J. Burns (corresponding author, burns@merl.com), C. Danielson (danielson@merl.com) and S. Di Cairano (dicairano@merl.com) are with Mitsubishi Electric Research Laboratories, 201 Broadway, Cambridge, MA 02139.

J. Zhou is with GE Global Research, One Research Circle, Niskayuna, NY 12309. He contributed to this study while working at Mitsubishi Electric Research Laboratories. email: junqiang.zhou@ge.com

† Authors contributed equally to this work.

Prior work on predictive control of multi-evaporator systems has exploited the repeated evaporators and associated mechanical elements to identify structure in the underlying model [5], and in fact, similar observations underpin the current work. This structure has led several groups to propose decentralized controller architectures [6], [7], motivated primarily by an effort to overcome computational challenges associated with centralized approaches. However, prior approaches consider only fixed-operation machines where the number of active evaporators does not change. In practice, however, many multi-evaporator systems often experience low heat loads in localized zones such that a particular evaporator no longer needs to provide cooling and should be shut off while the remaining evaporators continue to provide service. Despite the promising advantages of MPC for vapor compression systems, key challenges remain to extend the approach to a multi-evaporator system where individual evaporators can be turned on or off independently, *e.g.,* by closing the valves that allow refrigerant to enter the evaporator and shutting off the associated fan. Turning subsystems on or off alters the model of the plant dynamics, and therefore induces changes in the prediction model and number of regulated variables, actuators, sensors, and constraints. A structural change of this nature typically requires a separate controller for each machine configuration, where at each control cycle the appropriate controller is switched in at runtime [8], [9].

Recent work has extended Youla-Kucera parameterization to handle the addition or removal of actuators and sensors from the control system during online operation. This has been termed 'plug-and-play' (PnP) control [9]. The PnP MPC has also been developed for complex networks based on decentralized [10] and distributed [11] approaches, motivated by the time-varying network topology in which subsystems join or leave the network. These proposed approaches require a re-design of the controllers to guarantee stability in response to changing network conditions. Control reconfiguration was introduced in [12] for fault tolerance in distributed MPC, where proposed controllers are robust to the worst-case coupling and thus need not be redesigned when faults are detected.

Control re-design for MPC typically requires either complex numerical procedures [13], [14] (solution of linear matrix inequalities, Riccati equations, etc.), which in turn require complex numerical algorithms, or deployment of large pre-designed sets of controller parameters into the hardware. It is impractical to implement such algorithms on vapor compressor machines with microprocessors having limited computational capabilities and memory. To address this shortcoming, this paper proposes a *reconfigurable* MPC design that exploits

the repeated subsystem model structure that emerges from multiple evaporators connected in parallel to a compressor and condenser (see Fig. 1). The proposed approach features a single "master" controller designed and tuned for the configuration where all subsystems are turned on, and enables automatic reconfiguration of the controller by simple operations for configurations when any number of evaporators are turned off. In this way, a master controller can be designed and tuned based on a single appropriately-partitioned prediction model, and using the proposed reconfiguration method, scale to any combination of active evaporators in a multi-evaporator VCS.

The paper is organized as follows: A description of the plant to be controlled is provided in Section II, which includes a description of the multi-evaporator VCS dynamics, constraints, control objectives and structure of the configuration-dependent model. The reconfigurable MPC is proposed in Section III, which discusses the plant model augmentations for the MPC prediction model and provides a design procedure for computing terminal cost and controller matrices that are amenable to online reconfiguration, as well as a detailed stability and feasibility analysis for the closed-loop system under a given configuration. In Section IV, a description is provided of the laboratory used to experimentally validate reconfigurable MPC, followed by a comparative simulation study between reconfigurable MPC and collection of individually-designed MPC controllers, and these simulated results are further confirmed with experiments. More advanced experiments are presented in Section V, including an extension of the method wherein autonomous reconfiguration is experimentally validated. Finally, concluding remarks are offered in Section VI.

Notation

$\mathbb{R}$ and $\mathbb{Z}$ denote the set of real and integer numbers, respectively. The interior of a set $\mathcal{X} \subseteq \mathbb{R}^n$ is denoted by $\mathrm{int}\,(\mathcal{X})$. The vector formed by concatenating $x \in \mathbb{R}^n$ and $y \in \mathbb{R}^m$ is denoted by $\mathrm{col}(x, y) \in \mathbb{R}^{n+m}$. The weighted squared 2-norm is denoted by $\|x\|_P^2 := x'Px$. $I \in \mathbb{R}^{n\times n}$ and $0 \in \mathbb{R}^{n\times m}$ denote the identity and the all-zero matrices of appropriate dimension n and m, respectively. Inequalities are component-wise, and $\prec$ and $\succ$ ($\preceq$ and $\succeq$) indicate positive and negative (semi)definiteness. For a matrix A, $\rho(A)$ is the spectral radius, i.e., the maximum of the absolute value of the eigenvalues, and A is Schur when $\rho(A)1$. A continuous-time signal $x(\tau)$ sampled with period T_s is denoted by the discrete-time signal $x(t) = x(tT_s)$ where $t \in \mathbb{Z}$. $x_{k|t}$ denotes the k-steps predicted value of x at time t. The block-diagonal matrix composed of sub-matrices $A_1, \ldots, A_N$ is denoted by

$$\mathrm{diag}(\{A_i\}_{i=1}^N) = \begin{bmatrix} A_1 & & \\ & \ddots & \\ & & A_N \end{bmatrix}.$$

The dense matrix composed of sub-matrices A_{ij} for $i = 1, \ldots, N$ and $j = 1, \ldots, M$ is denoted by

$$\mathrm{mat}(\{A_{ij}\}_{i=1,j=1}^{N,M}) = \begin{bmatrix} A_{11} & \cdots & A_{1M} \\ \vdots & \ddots & \vdots \\ A_{N1} & \cdots & A_{NM} \end{bmatrix}$$

II. Multi-Evaporator Vapor Compression System

This section describes the dynamics, constraints, control objectives and configurations of the Multi-Evaporator Vapor Compression System (ME-VCS) shown in Fig. 1.

A. ME-VCS Dynamics

The ME-VCS is comprised of a single outdoor unit and N indoor units. When operating in cooling mode, the outdoor unit receives low pressure, low temperature refrigerant in the vapor state from the indoor units. The compressor performs work to increase the pressure and temperature of the refrigerant. The amount of work done is controlled by the compressor rotational frequency CF. A sensor measures the discharge temperature Td of the refrigerant leaving the compressor. The refrigerant then flows through the outdoor heat exchanger across which a fan forces air. This removes heat from the refrigerant and causes it change phase from vapor to a saturated liquid. The amount of heat removed from the refrigerant depends on the outdoor air temperature OAT and outdoor fan speed ODF. In cooling mode, the outdoor unit heat exchanger acts as a condenser, and the phase change of the refrigerant in the condenser is assumed to be isobaric and occurs at a constant condensing temperature Tc which is measured by a sensor on the heat exchanger.

The dynamics of the vapor compression system over the full range of operating conditions are nonlinear, however changes around a particular operating point can be modeled with linear difference equations, and a controller designed using these linear models is able to satisfy the control objectives stated subsequently. Therefore we approximate the ME-VCS dynamics as linear, and this approach will be justified in experiments in Section IV. Accordingly, the dynamics of the outdoor unit are modeled by

$$x_0(t+1) = A_{00}x_0(t) + \sum_{j=0}^{N} B_{0j}u_j(t) \tag{1a}$$

$$y_0(t) = C_{00}^y x_0(t) + w_0(t) \tag{1b}$$

where the inputs $u_0 = \mathrm{col}(\mathrm{CF}, \mathrm{ODF}) \in \mathbb{R}^{m_0}$ are the compressor frequency CF and outdoor fan speed ODF, and the outputs $y_0 = \mathrm{col}(\mathrm{Td}, \mathrm{Te}, \mathrm{Tc})$ are the discharge Td, evaporator Te, and condenser Tc temperatures. The inputs u_j, $j = 1, \ldots, N$ pertain to the individual indoor units and are described below. The model is fit to input-output data, and thus the state of the outdoor unit $x_0(t) \in \mathbb{R}^{n_0}$ is non-physical. The discrete-time model (1) describes the ME-VCS system when sampled with a period of 1 minute.

An additive output disturbance $w_0(t)$ is used to capture the effects of outdoor air temperature OAT on the measured outputs $y_0(t)$. Since the outdoor air temperature varies with a diurnal period, we treat the disturbance $w_0(t)$ as constant on the time scale of the model (1),

$$w_0(t+1) = w_0(t). \tag{1c}$$

The ME-VCS has N indoor units indexed by $i \in \mathcal{I} = \{1, \ldots, N\}$. High pressure liquid refrigerant from the outdoor unit is routed to the indoor units. The amount of refrigerant that enters the indoor unit is controlled by the opening position

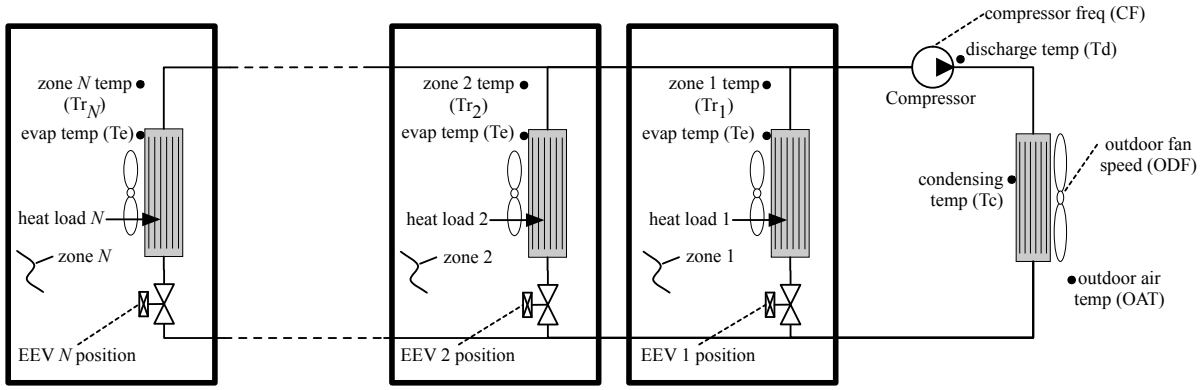

Fig. 1. Refrigerant piping arrangement of a multi-evaporator vapor compression system. The main actuators in the system are (i) the compressor, (ii) the outdoor (condenser) fan (ODF), and (iii) N electronic expansion valves (EEV). Sensors provide measurements of the compressor discharge temperature (Td), the evaporating temperature (Te), the condensing temperature (Tc) and the zone temperatures (Tri).

EEV_i of an electronic expansion valve. If the electronic expansion valve is open ($\text{EEV}_i > 0$), then refrigerant flows into the i-th indoor unit. As the refrigerant flows through the expansion valve, it experiences a rapid drop in pressure and temperature and changes state into a two-phase mixture of liquid and vapor. The low temperature two-phase refrigerant then flows through the indoor unit heat exchanger. A fan forces air from the zone across the heat exchanger, which absorbs heat from the zone. For the system considered, zone occupants can directly specify fan speed for personal comfort, therefore we do not consider the fan speed as an input available to the controller. An unmeasured heat load acts in each zone. Depending on the relative magnitude of the heat load and the heat removed by the indoor unit, the temperature in the zone Tr_i may be maintained, increased or decreased. The heat absorbed by each indoor unit causes the refrigerant to evaporate from a two-phase mixture to a saturated vapor. The phase change is assumed to be isobaric and occurs at a constant evaporating temperature Te, which is measured by sensors on the indoor unit heat exchangers.

Remark 1. *The entire ME-VCS is characterized by a single evaporating temperature due to the arrangement of valves shown in Fig. 1. In particular the ME-VCS considered does not include valves at the outlet of each indoor unit. Thus, all indoor units with open valves are at the same pressure and therefore the same evaporating temperature. As a consequence, the evaporator temperature Te is modeled as an output of the outdoor unit* (1b) *and depends only on the state x_0 of the outdoor unit.*

Since the effect of the electronic expansion valve position EEV_i on the room temperature Tr_i is nonlinear, each indoor unit has an inner feedback loop that manipulates the expansion valve position EEV_i to achieve a desired cooling capacity CCC_i. The cooling capacity is the amount of heat removed from the zone by the corresponding evaporator per unit time. The cooling capacity controllers linearize the response from the reference cooling capacity command of each zone CCC_i to the associated zone temperature Tr_i. Additional details on the inner feedback loops are provided in [15].

The dynamics of the i-th indoor unit, $i = 1, \ldots, N$, are modeled by

$$x_i(t+1) = A_{ii}x_i(t) + A_{i0}x_0(t) + \sum_{j=0}^{N} B_{ij}u_i(t) \quad (1d)$$

$$y_i(t) = C^y_{ii}x_i(t) + w_i(t) \quad (1e)$$

where the input $u_i = \text{CCC}_i \in \mathbb{R}^{m_i}$ is the cooling capacity command and the output $y_i = \text{Tr}_i \in \mathbb{R}$ is the zone temperature. The state of the i-th indoor unit $x_i \in \mathbb{R}^{n_i}$ is non-physical. The dynamics of the indoor unit depend on the state x_0 and input u_0 of the outdoor unit, as well as the inputs u_i for $i = 1, \ldots, N$ for each of the indoor units.

An additive output disturbance $w_i(t)$ is used to account for the effects of the heat load on the zone temperature $y_i(t)$. On the time scale of the discrete-time model (1d), we consider the heat load to be a constant disturbance

$$w_i(t+1) = w_i(t). \quad (1f)$$

The model (1) was experimentally identified with the structure described above for the ME-VCS operating under typical conditions as described in Section IV-A. The signals $u_i(t)$, $y_i(t)$, and $w_i(t)$ for $i \in \mathcal{I}_0 = \{0, \ldots, N\}$ are the deviations of the inputs, outputs, and disturbance from their nominal values, respectively. The physical meaning of the inputs, outputs, and disturbances in the ME-VCS model (1) are summarized in Table I. The model (1) has been reduced using standard Hankel singular value model reduction techniques and therefore is a minimal realization of the dynamics of the ME-VCS. The pairs (A_{ii}, B_{ii}) and (A_{ii}, C^y_{ii}) are controllable and observable, respectively, for $i = 0, \ldots, N$.

B. ME-VCS Constraints

This section describes the constraints on outputs, states, and inputs of the multi-evaporator vapor compression system.

The discharge, evaporating and condensing temperatures are constrained to protect the equipment. Physical damage to the compressor motor can occur when its internal temperature exceeds some critical value, thus we have an upper-bound $\text{Td}_{\max}$ on the compressor discharge temperature $\text{Td} \leq \text{Td}_{\max}$. If the indoor unit evaporators become too cold, frost can accumulate on the heat exchanger inhibiting heat transfer, thus

TABLE I
DEFINITION OF PHYSICAL SIGNALS

Type	Symbol	Description	Units
Inputs	u_0	Compressor Frequency (CF) Outdoor Fan Speed (ODF)	Hz rpm
	u_i	Cooling Capacity Command to i-th Zone (CCC_i)	%
Outputs	y_0	Discharge Temp (Td) Evaporating Temp (Te) Condensing Temp (Tc)	°C °C °C
	y_i	i-th Zone Temp (Tr_i)	°C
Disturbances	w_0	Temp offset due to Outdoor Air Temp (OAT)	°C
	w_i	Temp offset due to heat load in i-th Zone (Q_i)	°C
References	r_0 r_i	Discharge Temp Ref (Td ref) i-th Zone Temp Ref (Tr_i ref)	°C °C

we have a lower-bound $\text{Te}_{\min}$ on the evaporating temperature $\text{Te} \geq \text{Te}_{\min}$. Additionally, excessive condenser-side pressures (as measured through the surrogate condensing temperature) can rupture components of the equipment, and thus we have an upper-bound $\text{Tc}_{\max}$ on the condenser temperature $\text{Tc} \leq \text{Tc}_{\max}$. Finally, the liquid component of a two-phase mixture of refrigerant entering the compressor can damage mechanical elements within the compressor, and therefore we ensure that the state of the refrigerant entering the compressor is superheated vapor by enforcing a lower bound $\text{Tdsh}_{\min}$ on the compressor discharge superheat temperature $\text{Tdsh} \geq \text{Tdsh}_{\min}$, where $\text{Tdsh} := \text{Td} - \text{Tc}$.

Note that the output constraints only apply to the outputs (1b) of the outdoor unit. The outputs (1e) of the indoor units are unconstrained. In particular, the evaporating temperature constraint, which physically relates to the indoor units, is modeled as an output of the outdoor unit for reasons described in Remark 1. Thus, we define $\mathcal{Y}_0$ as the set of outputs of the outdoor unit y_0 that satisfy the output constraints

$$\mathcal{Y}_0 = \left\{ y_0 : \begin{bmatrix} -\infty \\ \text{Te}_{\min} \\ -\infty \\ \text{Tdsh}_{\min} \end{bmatrix} \leq y_0 \leq \begin{bmatrix} \text{Td}_{\max} \\ \infty \\ \text{Tc}_{\max} \\ \infty \end{bmatrix} \right\}.$$

Since the outputs Td, Te, Tc, and Tdsh are the deviations of the discharge, evaporating, condensing and discharge superheat temperatures from their nominal values, we have $\text{Td}_{\max}, \text{Tc}_{\max} > 0$, and $\text{Te}_{\min}, \text{Tdsh}_{\min} < 0$. Thus the output set $\mathcal{Y}_0$ contains the origin in its interior $0 \in \text{int}(\mathcal{Y}_0)$. The output constraints can be written as a constraint set on the outdoor unit state $x_0(t)$ parameterized by the outdoor unit disturbance $w_0(t)$

$$\mathcal{X}_0(w_0) = \Big\{ x_0 : C_{00} x_0 + w_0 \in \mathcal{Y}_0 \Big\}. \tag{2a}$$

We define $\mathcal{X} = \mathcal{X}_0 \times \mathbb{R}^{\sum_{i=1}^{N} n_i}$ as the state constraint set for the composite state $x = \text{col}(x_0, x_1, \ldots, x_N)$.

The outdoor unit has lower and upper bounds on the compressor frequency $\text{CF}_{\min} \leq \text{CF} \leq \text{CF}_{\max}$ and outdoor fan speed $\text{ODF}_{\min} \leq \text{ODF} \leq \text{ODF}_{\max}$. We define $\mathcal{U}_0$ as the set of inputs u_0 to the outdoor unit that satisfy the constraints

$$\mathcal{U}_0 = \left\{ u_0 : \begin{bmatrix} \text{CF}_{\min} \\ \text{ODF}_{\min} \end{bmatrix} \leq u_0 \leq \begin{bmatrix} \text{CF}_{\max} \\ \text{ODF}_{\max} \end{bmatrix} \right\}. \tag{2b}$$

Since the compressor frequency input CF is the deviation of the compressor frequency from its nominal value, we have $\text{CF}_{\min} < 0 < \text{CF}_{\max}$. Likewise $\text{ODF}_{\min} < 0 < \text{ODF}_{\max}$. Thus the input set $\mathcal{U}_0$ contains the origin in its interior, $0 \in \text{int}(\mathcal{U}_0)$.

Since the cooling capacity commands represent a fraction of the total rated cooling capacity of each evaporator [15], the inputs to the indoor units have lower and upper bounds $\text{CCC}_{i,\min} \leq \text{CCC}_i \leq \text{CCC}_{i,\max}$. We define $\mathcal{U}_i$ as the set of inputs u_i to the i-th indoor unit that satisfy the constraints

$$\mathcal{U}_i = \big\{ u_i : \ \text{CCC}_{i,\min} \leq u_i \leq \text{CCC}_{i,\max} \ \big\} \tag{2c}$$

where $\text{CCC}_{i,\min} < 0 < \text{CCC}_{i,\max}$. Thus the set $\mathcal{U}_i$ contains the origin in its interior $0 \in \text{int}(\mathcal{U}_i)$. We define $\mathcal{U} = \mathcal{U}_0 \times \mathcal{U}_1 \times \cdots \times \mathcal{U}_N$ as the input constraint set for the composite input $u = \text{col}(u_0, u_1, \ldots, u_N)$.

The system also has constraints on the amount the inputs can change during each sample period. The outdoor unit has constraints on the change in compressor frequency $\Delta\text{CF}_{\min} \leq \Delta\text{CF} \leq \Delta\text{CF}_{\max}$ and outdoor fan speed $\Delta\text{ODF}_{\min} \leq \Delta\text{ODF} \leq \Delta\text{ODF}_{\max}$. We define $\Delta\mathcal{U}_0$ as the set of admissible changes $\Delta u_0(t) = u_0(t) - u_0(t-1)$ to the inputs to the outdoor unit

$$\Delta\mathcal{U}_0 = \left\{ \Delta u_0 : \begin{bmatrix} \Delta\text{CF}_{\min} \\ \Delta\text{ODF}_{\min} \end{bmatrix} \leq \Delta u_0 \leq \begin{bmatrix} \Delta\text{CF}_{\max} \\ \Delta\text{ODF}_{\max} \end{bmatrix} \right\}. \tag{2d}$$

The set $\Delta\mathcal{U}_0$ contains the origin in its interior $0 \in \text{int}(\Delta\mathcal{U}_0)$ since the change in actuators can be positive or negative $\Delta\text{CF}_{\min} \leq 0 \leq \Delta\text{CF}_{\max}$ and $\Delta\text{ODF}_{\min} \leq 0 \leq \Delta\text{ODF}_{\max}$.

The indoor units have inner feedback loops that control the position of the electronic expansion valves to track the cooling capacity command. The change in cooling capacity command is bounded $\Delta\text{CCC}_{i,\min} \leq \Delta\text{CCC}_i \leq \Delta\text{CCC}_{i,\max}$ to ensure that the transient response of the inner-loop controllers settles during the sample period. We define $\Delta\mathcal{U}_i$ as the set of admissible changes $\Delta u_i(t) = u_i(t) - u_i(t-1)$ to the input of the i-th indoor unit

$$\Delta\mathcal{U}_i = \big\{ \Delta u_i : \ \Delta\text{CCC}_{i,\min} \leq \Delta u_i \leq \Delta\text{CCC}_{i,\max} \ \big\}. \tag{2e}$$

The set $\Delta\mathcal{U}_i$ contains the origin in its interior $0 \in \text{int}(\Delta\mathcal{U}_i)$ since $\Delta\text{CCC}_{i,\min} < 0 < \Delta\text{CCC}_{i,\max}$.We define $\Delta\mathcal{U} = \Delta\mathcal{U}_0 \times \Delta\mathcal{U}_1 \times \cdots \times \Delta\mathcal{U}_N$ as constraint set for the composite change in input $\Delta u = \text{col}(\Delta u_0, \Delta u_1, \ldots, \Delta u_N)$.

C. ME-VCS Configuration-Dependent Model

An indoor unit is said to be active when its associated expansion valve is open allowing refrigerant to flow through the evaporator providing cooling. Conversely, an indoor unit is said to be inactive when its associated expansion valve is closed and no cooling occurs. A configuration of the ME-VCS is a combination of active and inactive indoor units. In

this section we describe our configuration-dependent model of the ME-VCS.

To each indoor unit $i \in \mathcal{I}$ we assign a configuration variable $\varsigma_i \in \{0,1\}$ where $\varsigma_i = 1$ if the unit is active and $\varsigma_i = 0$ if the unit is inactive. The configuration of the entire ME-VCS is given by the vector $\varsigma = \mathrm{col}(\varsigma_0, \varsigma_1, \ldots, \varsigma_N)$ where $\varsigma_0 = 1$ since the outdoor unit is always active. The configuration $\varsigma \in \{1\} \times \{0,1\} \times \cdots \times \{0,1\}$ is used to obtain a parameter-dependent controller [14] which operates for any ME-VCS configuration. In the subsequent analysis, the configuration is assumed to be kept constant, at least for a sufficiently long dwell time.

For configuration ς, the dynamics of the outdoor unit are modeled by

$$x_0(t+1) = A_{00}x_0(t) + \sum\nolimits_{j=0}^{N} \varsigma_j B_{0j} u_j(t) \tag{3a}$$

where the future state $x_0(t+1)$ of the outdoor unit is only affected by the inputs $u_j(t)$ of active units $\varsigma_j = 1$. The dynamics of the i-th indoor unit are modeled by

$$x_i(t+1) = A_{ii}x_i(t) + \varsigma_i A_{i0}x_0(t) + \sum_{j=0}^{N} \varsigma_i\varsigma_j B_{ij}u_j(t) \tag{3b}$$

If the i-th indoor unit is inactive $\varsigma_i = 0$, then its future state $x_i(t+1)$ depends only on its current state $x_i(t)$. If the i-th indoor unit is active $\varsigma_i = 1$, then its future state $x_i(t+1)$ also depends on the outdoor unit state $x_0(t)$ and the inputs $u_j(t)$ to the other active indoor units $\varsigma_j = 1$.

The state $x_i(t)$ and zone temperature $y_i(t)$ of inactive units $\varsigma_i = 0$ will converge to some equilibrium values for a constant, finite heat load $|w_i|\infty$. Thus, since (3) is a minimal realization of the ME-VCS dynamics, the dynamics matrix A_{ii} of the i-th indoor unit is Schur, $\rho(A_{ii})1$.

The configuration-dependent model (3) can be written more compactly in the form

$$x(t+1) = A^{\varsigma}x(t) + B^{\varsigma}u(t) \tag{4}$$

where $x = \mathrm{col}(x_0, x_1, \ldots, x_N)$ and $u = \mathrm{col}(u_0, u_1, \ldots, u_N)$ are the composite state and input respectively. The state-update matrix A^{ς} is block lower-arrowhead and the input matrix B^{ς} is dense, given by

$$A^{\varsigma} = \begin{bmatrix} A_{00} & & & \\ \varsigma_1 A_{10} & A_{11} & & \\ \vdots & & \ddots & \\ \varsigma_N A_{N0} & & & A_{NN} \end{bmatrix}, \quad B^{\varsigma} = \mathrm{mat}(\{\varsigma_i\varsigma_j B_{ij}\}_{i,j\in\mathcal{I}_0})$$

The structure of the state-update matrix A reflects the one-way coupling between the state x_0 of the outdoor unit and the states x_i of the indoor units [16]. The reconfigurable controller described in the next section will exploit the block lower-arrowhead structure of the A^{ς} matrix to guarantee stability in different configurations. We assume that the pair $(A^{\varsigma}, B^{\varsigma})$ is controllable for every configuration ς.

D. Control Objectives

The control objectives are to regulate the discharge and zone temperatures to desired reference values while satisfying the constraints in the presence of persistent disturbances. In particular, the compressor discharge temperature Td is regulated to a setpoint $\mathrm{Td}_{\mathrm{ref}}$ determined for optimal energy efficiency. The zone temperatures Tr_i are regulated to setpoints $\mathrm{Tr}_{i,\mathrm{ref}}$ provided by an external source such as a thermostat.

Further, we aim to design a single controller that can be easily reconfigured and achieves these control objectives for every configuration of the ME-VCS. This avoids the computational complexity of designing and storing separate controllers for each possible configuration. To achieve these objectives, the following section develops a configuration-dependent ME-VCS model and details its structure for control design.

III. Reconfigurable Control Design

In this section we present a reconfigurable model predictive controller for the configuration-dependent ME-VCS. First, we augment the model (4) of the ME-VCS to provide the desired steady-state behavior. Then, we present a reconfigurable linear controller that achieves the control objectives in the absence of constraints. Finally, we present a reconfigurable model predictive controller that achieves the control objective while satisfying constraints.

A. Augmentations of the ME-VCS Model

In this section we describe augmentations to the configuration-dependent plant model (3) that capture the control objectives described in Section II-D.

We define reference signals $r_0 = \mathrm{Td}_{\mathrm{ref}}$ and $r_i = \mathrm{Tr}_{i,\mathrm{ref}}$ for the discharge and zone temperature setpoints. The energy-optimal discharge temperature reference is a linear function of the compressor frequency CF (control input) and the outdoor air temperature OAT (disturbance input) [17] given by

$$r_0 = E_{00}u_0 + G_{00}w_0 \tag{5}$$

where the coefficients E_{00}, G_{00} are experimentally characterized to minimize power consumption over a range of operating conditions. Since w_0 is constant in prediction (1c), the prediction model of the reference discharge temperature is given by

$$r_0(t+1) = r_0(t) + E_{00}\Delta u_0(t). \tag{6a}$$

The reference zone temperatures are assumed constant and modeled by

$$r_i(t+1) = r_i(t), \tag{6b}$$

for $i = 1, \ldots, N$. For consistency we define $E_{ii} = 0$ and $G_{ii} = 0$ for $i \in \mathcal{I}$. Thus, the composite reference $r = \mathrm{col}(r_0, r_1, \ldots, r_N)$ is modeled by

$$r(t+1) = r(t) + E\Delta u_0(t)$$

where $E = \mathrm{col}(E_{00}, E_{11}, \ldots, E_{NN})$ and $G = \mathrm{col}(G_{00}, G_{11}, \ldots, G_{NN})$.

The compressor discharge temperature and zone room temperatures are defined as performance outputs

$$z_0(t) = C_{00}x_0(t) + D_{00}w_0(t) \tag{6c}$$

$$z_i(t) = C_{ii}x_i(t) + D_{ii}w_i(t) \tag{6d}$$

where $z_0 = \text{Td} \in \mathbb{R}^{p_0}$ is the discharge temperature and $z_i = \text{Tr}_i \in \mathbb{R}^{p_i}$ for $i = 1, \dots, N$ are the zone temperatures. The output additive disturbances $w_0(t)$ and $w_i(t)$ are constant (1c) and (1f). The zone temperature tracking errors $z_i(t) - r_i$ are integrated

$$\xi_i(t+1) = \varsigma_i \xi_i(t) + \varsigma_i \big(z_i(t) - r_i(t)\big) \tag{6e}$$

for $i = 1, \dots, N$. The integrators (6e) provide integral action and hence zero steady-state tracking error in the presence of uncertainties in zone volume and heat loads. Although the auxiliary output offset (1c) and (1f) provide offset-free tracking [18], [19], our experimental results have shown that combining both integral action and output offsets provides improved transient performance. Note that when the i-th indoor unit is inactive $\varsigma_i = 0$ the corresponding integrator is shut-off $\xi_i(t+1) = 0$.

The control objectives require that the controller enforces constraints. Since the ME-VCS has constraints (2d) and (2e) on the change in input, we use incremental inputs [20]

$$u_i(t) = \varsigma_i u_i(t-1) + \varsigma_i \Delta u_i(t) \tag{6f}$$

for the outdoor $i = 0$ and indoor $i = 1, \dots, N$ units. This also ensures that the steady-state incremental input $\Delta u_i(t) \to 0$ approaches zero when tracking a constant reference with constant disturbances. Note that when the i-th indoor unit is inactive $\varsigma_i = 0$ equation (6f) sets the input $u_i(t)$ to zero, and the associated inner feedback loop closes the expansion valve.

It will be convenient to combine the ME-VCS model (3) and the model augmentations (6) into a single configuration-dependent model. The augmented state of the outdoor unit $\hat{x}_0 = \text{col}(x_0, u_0)$ includes the outdoor unit state x_0 and input u_0. The augmented output $\hat{z}_0 = z_0 - r_0$ is the difference between the discharge temperature $z_0 = \text{Td}$ and its reference $r_0 = \text{Td}_{\text{ref}}$. The augmented state of the i-th indoor unit $\hat{x}_i = \text{col}(x_i, u_i, \xi_i)$ includes the indoor unit state x_i, input u_i, and integrator ξ_i. The augmented output $\hat{z}_i = \text{col}(z_i - r_i, \xi_i)$ includes the room tracking error $z_i - r_i = \text{Tr}_i - \text{Tr}_{i,\text{ref}}$ and its integral ξ_i. The augmented dynamics are modeled by

$$\hat{x}(t+1) = \hat{A}^\varsigma \hat{x}(t) + \hat{B}^\varsigma \Delta u(t) + \hat{B}^\varsigma_w w(t) + \hat{B}^\varsigma_r r(t) \tag{7a}$$

$$\hat{z}(t) = \hat{C}^\varsigma \hat{x}(t) + \hat{D}_w w(t) + \hat{D}_r r(t) \tag{7b}$$

where $\hat{x} = \text{col}(\hat{x}_0, \hat{x}_1, \dots, \hat{x}_N)$ and $\hat{z} = \text{col}(\hat{z}_0, \hat{z}_1, \dots, \hat{z}_N)$ are the augmented state and performance outputs respectively, $\Delta u = \text{col}(\Delta u_0, \Delta u_1, \dots, \Delta u_N)$ are the incremental inputs, $r = \text{col}(r_0, r_1, \dots, r_N)$ are the references, and $w = \text{col}(w_0, w_1, \dots, w_N)$ are the disturbances. The dense state-update matrix $\hat{A}^\varsigma = \text{mat}(\{\hat{A}_{ij}\}_{i,j=0}^N)$ is comprised of the sub-matrices

$$\hat{A}^\varsigma_{00} = \left[\begin{smallmatrix} A_{00} & B_{00} \\ 0 & I \end{smallmatrix}\right], \ \hat{A}^\varsigma_{0j} = \left[\begin{smallmatrix} 0 & B_{0j} & 0 \\ 0 & 0 & 0 \end{smallmatrix}\right],$$

$$\hat{A}^\varsigma_{i0} = \begin{bmatrix} 0 & B_{i0} \\ 0 & 0 \\ 0 & 0 \end{bmatrix}, \ \hat{A}^\varsigma_{ii} = \begin{bmatrix} A_{ii} & \varsigma_i B_{ii} & 0 \\ 0 & \varsigma_i I & 0 \\ \varsigma_i C_{ii} & 0 & \varsigma_i I \end{bmatrix}, \ \hat{A}^\varsigma_{ij} = \begin{bmatrix} 0 & \varsigma_i \varsigma_j B_{ij} & 0 \\ 0 & 0 & 0 \\ 0 & 0 & 0 \end{bmatrix}$$

for $i \neq j \in \mathcal{I}$. The input matrices are given by $\hat{B}^\varsigma = \text{mat}\big(\{\hat{B}^\varsigma_{ij}\}_{i,j \in \mathcal{I}_0}\big)$, $\hat{B}_r = \text{diag}(\hat{B}_{r,00}, \dots, \hat{B}_{r,NN})$, and $\hat{B}_w = \text{diag}(\hat{B}_{w,00}, \dots, \hat{B}_{w,NN})$ where

$$\hat{B}^\varsigma_{ii} = \begin{bmatrix} B^\varsigma_{ii} \\ \varsigma_i I \\ 0 \end{bmatrix}, \hat{B}^\varsigma_{ij} = \begin{bmatrix} B^\varsigma_{ij} \\ 0 \\ 0 \end{bmatrix}, \hat{B}^\varsigma_{r,ii} = \begin{bmatrix} 0 \\ 0 \\ -\varsigma_i I \end{bmatrix}, \hat{B}^\varsigma_{w,ii} = \begin{bmatrix} 0 \\ 0 \\ \varsigma_i D \end{bmatrix}.$$

The output matrices are block diagonal and given by $\hat{C}^\varsigma = \text{diag}(\hat{C}_{00}, \dots, \hat{C}_{NN})$, $\hat{D}^\varsigma_w = \text{diag}(\hat{D}_{w,00}, \dots, \hat{D}_{w,NN})$, and $\hat{D}^\varsigma_r = \text{diag}(\hat{D}_{r,00}, \dots, \hat{D}_{r,NN})$ where $\hat{C}^\varsigma_{00} = \left[\begin{smallmatrix} C_{00} & 0 \end{smallmatrix}\right]$, $\hat{D}^\varsigma_{w,00} = D_{w,00}$, $\hat{D}_{r,00} = -I$, and

$$\hat{C}^\varsigma_{ii} = \left[\begin{smallmatrix} \varsigma_i C_{ii} & 0 & 0 \\ 0 & 0 & I \end{smallmatrix}\right], \ \hat{D}^\varsigma_{w,ii} = \left[\begin{smallmatrix} \varsigma_i D_{w,ii} \\ 0 \end{smallmatrix}\right], \ \hat{D}_{r,ii} = \left[\begin{smallmatrix} -\varsigma_i I \\ 0 \end{smallmatrix}\right].$$

Although the matrices are dense, the following proposition reveals important configuration-dependent structure of the augmented model (7).

Proposition III.1. *For configuration ς, let $\mathcal{A} = \{i \in \mathcal{I}_0 : \varsigma_i = 1\}$ be the set of active units and $\mathcal{N} = \{i \in \mathcal{I} : \varsigma_i = 0\}$ be the set of inactive units. Then, the model* (7) *can be written as*

$$\begin{bmatrix} \hat{x}_\mathcal{A}(t+1) \\ \hat{x}_\mathcal{N}(t+1) \end{bmatrix} = \begin{bmatrix} \hat{A}_{\mathcal{A}\mathcal{A}} & 0 \\ 0 & \hat{A}_{\mathcal{N}\mathcal{N}} \end{bmatrix} \begin{bmatrix} \hat{x}_\mathcal{A}(t) \\ \hat{x}_\mathcal{N}(t) \end{bmatrix} + \begin{bmatrix} \hat{B}_{\mathcal{A}\mathcal{A}} & 0 \\ 0 & 0 \end{bmatrix} \begin{bmatrix} \Delta u_\mathcal{A}(t) \\ \Delta u_\mathcal{N}(t) \end{bmatrix} \tag{8a}$$
$$+ \begin{bmatrix} \hat{B}_{w,\mathcal{A}\mathcal{A}} & 0 \\ 0 & 0 \end{bmatrix} \begin{bmatrix} w_\mathcal{A}(t) \\ w_\mathcal{N}(t) \end{bmatrix} + \begin{bmatrix} \hat{B}_{r,\mathcal{A}\mathcal{A}} & 0 \\ 0 & 0 \end{bmatrix} \begin{bmatrix} r_\mathcal{A}(t) \\ r_\mathcal{N}(t) \end{bmatrix}$$

$$\begin{bmatrix} \hat{z}_\mathcal{A}(t) \\ \hat{z}_\mathcal{N}(t) \end{bmatrix} = \begin{bmatrix} \hat{C}_{\mathcal{A}\mathcal{A}} & 0 \\ 0 & 0 \end{bmatrix} \begin{bmatrix} \hat{x}_\mathcal{A}(t) \\ \hat{x}_\mathcal{N}(t) \end{bmatrix} + \begin{bmatrix} \hat{D}_{w,\mathcal{A}\mathcal{A}} & 0 \\ 0 & 0 \end{bmatrix} \begin{bmatrix} w_\mathcal{A}(t) \\ w_\mathcal{N}(t) \end{bmatrix} + \tag{8b}$$
$$+ \begin{bmatrix} \hat{D}_{r,\mathcal{A}\mathcal{A}} & 0 \\ 0 & 0 \end{bmatrix} \begin{bmatrix} r_\mathcal{A}(t) \\ r_\mathcal{N}(t) \end{bmatrix}$$

Furthermore, for any configuration ς, we have the following properties:

1) *The dynamics of the inactive state $x_\mathcal{N}$ are stable* i.e.*, the matrix $\hat{A}_{\mathcal{N}\mathcal{N}}$ is Schur $\rho\big(\hat{A}_{\mathcal{N}\mathcal{N}}\big) < 1$.*
2) *The dynamics of the active state $x_\mathcal{A}$ are controllable* i.e.*, the pair $(\hat{A}_{\mathcal{A}\mathcal{A}}, \hat{B}_{\mathcal{A}\mathcal{A}})$ is controllable.*
3) *The dynamics of the active state $x_\mathcal{A}$ are observable* i.e.*, the pair $(\hat{A}_{\mathcal{A}\mathcal{A}}, \hat{C}_{\mathcal{A}\mathcal{A}})$ is observable.*
4) *The dynamics of the inactive state $x_\mathcal{N}$ are unobservable.*

The structure (8) of the augmented model (7) will be used to prove that the reconfigurable linear and model predictive controllers stabilize the ME-VCS for every configuration ς.

B. Desired Steady-State

At steady-state, the integrator states $\xi_i(\infty) = 0$ and incremental inputs $\Delta u_i(\infty) = 0$ should be zero indicating that the performance outputs (6c) track the desired reference values (6a) and (6b). However, the steady-state inputs $u_i(\infty) = u_i^\infty$ and states $x_i(\infty) = x_i^\infty$ for each unit $i = 0, \dots, N$ will depend on the values of the constant disturbances $w_i(t) = w_i^\infty$ and steady-state references $r_i(t) = r_i^\infty$ for $i = 0, \dots, N$. The equilibrium states x_i^∞ and inputs u_i^∞ are determined by solving

$$x^\infty = A^\varsigma x^\infty + B^\varsigma u^\infty \tag{9a}$$

$$r^\infty = C^\varsigma x^\infty + D^\varsigma_w w^\infty \tag{9b}$$

where $x^\infty = \text{col}(x_0^\infty, x_1^\infty, \dots, x_N^\infty)$, $u^\infty = \text{col}(u_0^\infty, u_1^\infty, \dots, u_N^\infty)$, $r^\infty = \text{col}(r_0^\infty, r_1^\infty, \dots, r_N^\infty)$, and $w^\infty = \text{col}(w_0^\infty, w_1^\infty, \dots, w_N^\infty)$ are the composite states, inputs, references, and disturbances, respectively. The composite matrices A^ς and B^ς are defined in (4) while $C^\varsigma = \text{diag}(\varsigma_0 C_{00}, \dots, \varsigma_N C_{NN})$ and $D^\varsigma_w = \text{diag}(\varsigma_0 D_{w,00}, \dots, \varsigma_N D_{w,NN})$. For steady state references r^∞, only $(r_1^\infty, \dots, r_N^\infty)$ are independent variables,

and r_0^∞ is a function given by $r_0^\infty = E_{00}u_0^\infty + G_{00}w_0^\infty$. Therefore, Equation (9) can be rewritten as

$$\begin{bmatrix} A^\varsigma - I & B^\varsigma \\ C^\varsigma & E^\varsigma \end{bmatrix} \begin{bmatrix} x^\infty \\ u^\infty \end{bmatrix} = \begin{bmatrix} 0 \\ D_r^\varsigma r^\infty + \bar{D}_w^\varsigma w^\infty \end{bmatrix} \tag{10}$$

where $E^\varsigma = \operatorname{diag}(\varsigma_0 E_{00}, \ldots, \varsigma_N E_{NN})$, $D_r^\varsigma = \operatorname{diag}(0, \varsigma_0 I, \ldots, \varsigma_N I)$, $\bar{D}_w^\varsigma = G^\varsigma - D_w^\varsigma$ and $G^\varsigma = \operatorname{diag}(\varsigma_0 G_{00}, \ldots, \varsigma_N G_{NN})$. Notice that we keep r_0^∞ in the vector r^∞ in (10) for notational consistency, and the corresponding entries in D_r^ς are set as zero.

Instead of finding x^∞, u^∞ corresponding to each given (w^∞, r^∞) by solving (10), we are interested in finding parameterized solutions $x^\infty = \Pi_w^\varsigma w^\infty + \Pi_r^\varsigma r^\infty$ and $u^\infty = \Gamma_w^\varsigma w^\infty + \Gamma_r^\varsigma r^\infty$ for $(w^\infty, r^\infty) \in \Omega_s^\varsigma$, where Ω_s^ς denotes the set of admissible constant disturbance inputs and references. Equation (10) can thus be written as

$$\begin{bmatrix} A^\varsigma - I & B^\varsigma \\ C^\varsigma & E^\varsigma \end{bmatrix} \begin{bmatrix} \Pi_w^\varsigma & \Pi_r^\varsigma \\ \Gamma_w^\varsigma & \Gamma_r^\varsigma \end{bmatrix} = \begin{bmatrix} 0 & 0 \\ \bar{D}_w^\varsigma & D_r^\varsigma \end{bmatrix} \tag{11}$$

Equation (11) is solvable if $\operatorname{rank} \left[\begin{smallmatrix} A^\varsigma - I & B^\varsigma \\ C^\varsigma & E^\varsigma \end{smallmatrix}\right] = \sum_{i=0}^N n_i + \sum_{i \in \mathcal{A}} p_i$ where $\mathcal{A}$ is the set of active units. Solutions to (11) are determined for a given configuration ς of the ME-VCS, and then the steady-state of the augmented states $\hat{x}^\infty = \operatorname{col}(\hat{x}_0^\infty, \hat{x}_1^\infty, \ldots, \hat{x}_N^\infty)$ in (7) can be derived in which it follows $\hat{x}_0^\infty = \operatorname{col}(x_0^\infty, u_0^\infty)$ and $\hat{x}_i^\infty = \operatorname{col}(x_i^\infty, u_i^\infty, 0)$ for $i = 1, \ldots, N$ since the integrator states $\xi_i(\infty) = 0$. The solutions $\hat{x}^\infty$ will be used to update the terminal cost in the reconfigurable model predictive controller. The set of admissible constant disturbance input and reference signals Ω_s^ς, in which desired constant outputs can be tracked without steady state error, are given by

$$\begin{aligned} \Omega_s^\varsigma = \big\{ (w^\infty, r^\infty) :\ & \Pi_w^\varsigma w^\infty + \Pi_r^\varsigma r^\infty \in \operatorname{int}\left(\mathcal{X}_0(w^\infty)\right), \\ & \Gamma_w^\varsigma w^\infty + \Gamma_r^\varsigma r^\infty \in \operatorname{int}\left(\mathcal{U}\right) \big\} \end{aligned} \tag{12}$$

C. Reconfigurable Linear Controller

In this section we present a procedure for designing a configuration-dependent linear controller that achieves the desired tracking objectives for the ME-VCS. The structure of the controller guarantees that the linear controller stabilizes the ME-VCS in every configuration ς. Such a reconfigurable linear controller will be used to design a reconfigurable model predictive controller in the next section.

We consider a configuration-dependent linear controller with the following structure

$$\begin{aligned} \Delta u_0(t) = \varsigma_0 \hat{K}_{00}\big(\hat{x}_0(t) - \hat{x}_0^\infty\big) + \\ + \textstyle\sum_{i=1}^N \varsigma_i \hat{K}_{0i}\big(\hat{x}_i(t) - \hat{x}_i^\infty\big) \end{aligned} \tag{13a}$$

$$\Delta u_i(t) = \varsigma_i \hat{K}_{ii}(\hat{x}_i(t) - \hat{x}_i^\infty) \tag{13b}$$

for $i = 1, \ldots, N$ where $\hat{x}_0^\infty = \operatorname{col}(x_0^\infty, u_0^\infty)$ and $\hat{x}_i^\infty = \operatorname{col}(x_i^\infty, u_i^\infty, 0)$ are the target equilibrium of the augmented states of the outdoor $\hat{x}_0$ and indoor $\hat{x}_i$ units respectively. The linear controller (13) can be written more compactly as $\Delta u(t) = \hat{K}^\varsigma(\hat{x}(t) - \hat{x}^\infty)$ where the gain $\hat{K}^\varsigma$ is given by

$$\hat{K}^\varsigma = \begin{bmatrix} \varsigma_0\hat{K}_{00} & \varsigma_1\hat{K}_{01} & \cdots & \varsigma_N\hat{K}_{0N} \\ 0 & \varsigma_1\hat{K}_{11} & & \\ \vdots & & \ddots & \\ 0 & & & \varsigma_N\hat{K}_{NN} \end{bmatrix}. \tag{14}$$

A configuration-dependent controller of the form (13) will be used to stabilize the configuration-dependent augmented system (7). The stability of the closed-loop system will be certified in Lemma III.2 by the existence of a configuration-dependent Lyapunov function $V(\hat{x}) = \hat{x}'\hat{P}^\varsigma\hat{x}$ where matrix $\hat{P}^\varsigma$ has a block diagonal structure

$$\hat{P}^\varsigma = \begin{bmatrix} \varsigma_0\hat{P}_0 & & \\ & \ddots & \\ & & \varsigma_N\hat{P}_N \end{bmatrix} \succeq 0 \tag{15}$$

where $\hat{P}^{\mathbf{1}} \succ 0$. The controller gain (14) and the matrix (15) are chosen to satisfy the discrete-time Lyapunov equation

$$\begin{aligned} (\hat{A}^{\mathbf{1}} + \hat{B}^{\mathbf{1}}\hat{K}^{\mathbf{1}})'\hat{P}^{\mathbf{1}}(\hat{A}^{\mathbf{1}} + \hat{B}^{\mathbf{1}}\hat{K}^{\mathbf{1}}) - \hat{P}^{\mathbf{1}} \\ \preceq -\hat{C}^{\mathbf{1}\prime}\hat{Q}^{\mathbf{1}}\hat{C}^{\mathbf{1}} - \hat{K}^{\mathbf{1}\prime}\hat{R}^{\mathbf{1}}\hat{K}^{\mathbf{1}} \end{aligned} \tag{16}$$

for the nominal configuration $\varsigma = \mathbf{1}$ where all units are active $\varsigma_i = 1$ for $i = 0, \ldots, N$. The structured matrices $\hat{Q}^\varsigma = \operatorname{diag}(\varsigma_0\hat{Q}_0, \ldots, \varsigma_N\hat{Q}_N) \succ 0$ and $\hat{R}^\varsigma = \operatorname{diag}(\varsigma_0\hat{R}_0, \ldots, \varsigma_N\hat{R}_N) \succ 0$ are used to shape the closed-loop behavior of the controller (13). In the next section $\hat{Q}^\varsigma$ and $\hat{R}^\varsigma$ will be the penalty matrices in the reconfigurable model predictive controller.

From (16) it can be shown that the configuration-dependent linear controller (13) stabilizes the configuration-dependent augmented system (7) when both are in the nominal configuration $\varsigma = \mathbf{1}$. This means that the linear controller (13) achieves the desired tracking objective $z_i(t) \to r_i^\infty$. The following lemma shows that this result holds for any configuration ς.

Lemma III.2. *Let* (14) *and* (15) *satisfy* (16). *Consider the configuration-dependent linear controller* (13) *in closed-loop with the configuration-dependent augmented model* (7). *Then*

1) *The closed-loop state $x_0(t) \to x_0^\infty$ and input $u_0(t) \to u_0^\infty$ of the outdoor unit converge to their desired equilibrium values. The discharge temperature $z_0(t) \to r_0^\infty$ converges to its reference value.*
2) *The closed-loop states $x_i(t) \to x_i^\infty$ and inputs $u_i(t) \to u_i^\infty$ of the active indoor units $\varsigma_i = 1$ converge to their desired equilibrium values. The room temperature $z_i(t) \to r_i^\infty$ converge to their reference values.*
3) *The closed-loop states $x_i(t)$ of the inactive indoor units $\varsigma_i = 0$ converges to zero. The room temperatures $z_i(t) \to D_{w,ii}w_i^\infty$ are bounded and converge to some steady-state temperature $D_{w,ii}w_i^\infty$ which depends on the constant heat load w_i^∞.*

Proof. For configuration ς let $\mathcal{A}$ and $\mathcal{N}$ be defined as in Proposition III.1. Define the augmented offset states

$$\tilde{x}_i = \begin{cases} \hat{x}_i - \hat{x}_i^\infty & \text{if } i \in \mathcal{A} \\ \hat{x}_i & \text{if } i \in \mathcal{N}. \end{cases}$$

Substituting the augmented offset states into the augmented dynamics (7) produces the linear system

$$\tilde{x}(t+1) = \hat{A}^\varsigma\tilde{x}(t) + \hat{B}^\varsigma\Delta u(t). \tag{17}$$

The offset dynamics (17) do not depend on the references and disturbances due to the definition (9) of the target equilibrium $\hat{x}^\infty$ and since the integrators (6e) are shut-off when a unit is

inactive, and the references (6a) and (6b), and disturbances (1c) and (1f) are constant. By definition of the offset states, the claims of Lemma III.2 are true if the controller (13) asymptotically stabilizes (17).

According to Proposition III.1 the offset model (17) has the structure

$$\begin{bmatrix} \tilde{x}_{\mathcal{A}}(t+1) \\ \tilde{x}_{\mathcal{N}}(t+1) \end{bmatrix} = \begin{bmatrix} \hat{A}_{\mathcal{A}\mathcal{A}} & 0 \\ 0 & \hat{A}_{\mathcal{N}\mathcal{N}} \end{bmatrix} \begin{bmatrix} \tilde{x}_{\mathcal{A}}(t) \\ \tilde{x}_{\mathcal{N}}(t) \end{bmatrix} + \begin{bmatrix} \hat{B}_{\mathcal{A}\mathcal{A}} 0 \\ 0 \ 0 \end{bmatrix} \begin{bmatrix} \Delta\tilde{u}_{\mathcal{A}}(t) \\ \Delta\tilde{u}_{\mathcal{N}}(t) \end{bmatrix} \quad (18a)$$

and the controller (13) has the structure

$$\begin{bmatrix} \Delta\tilde{u}_{\mathcal{A}}(t) \\ \Delta\tilde{u}_{\mathcal{N}}(t) \end{bmatrix} = \begin{bmatrix} \hat{K}^{\varsigma}_{\mathcal{A}\mathcal{A}} & 0 \\ 0 & 0 \end{bmatrix} \begin{bmatrix} \tilde{x}_{\mathcal{A}}(t) \\ \tilde{x}_{\mathcal{N}}(t) \end{bmatrix}. \quad (18b)$$

We will prove that the closed-loop system (18) is asymptotically stable using the quadratic Lyapunov function

$$V(\tilde{x}) = \begin{bmatrix} \tilde{x}_{\mathcal{A}} \\ \tilde{x}_{\mathcal{N}} \end{bmatrix}' \begin{bmatrix} \hat{P}_{\mathcal{A}} & 0 \\ 0 & S_{\mathcal{N}} \end{bmatrix} \begin{bmatrix} \tilde{x}_{\mathcal{A}} \\ \tilde{x}_{\mathcal{N}} \end{bmatrix}$$

where $\hat{P}_A = \operatorname{diag}(\{\hat{P}_i\}_{i\in\mathcal{A}}) \succ 0$ is the active part of the Lynapunov matrix (15) and $\mathcal{S}_N \succ 0$ will be specified later. Based on its structure, the closed-loop system (18) is asymptotically stable if the following Lyapunov equations are satisfied

$$(\hat{A}_{\mathcal{A}\mathcal{A}} + \hat{B}_{\mathcal{A}\mathcal{A}}\hat{K}_{\mathcal{A}\mathcal{A}})'\hat{P}_{\mathcal{A}}(\hat{A}_{\mathcal{A}\mathcal{A}} + \hat{B}_{\mathcal{A}\mathcal{A}}\hat{K}_{\mathcal{A}\mathcal{A}}) - \hat{P}_{\mathcal{A}} \prec 0 \quad (19a)$$

$$\hat{A}'_{\mathcal{N}\mathcal{N}} S_{\mathcal{N}} \hat{A}_{\mathcal{N}\mathcal{N}} - S_{\mathcal{N}} \prec 0. \quad (19b)$$

By Proposition III.1, there exists a matrix $\mathcal{S}_N \succ 0$ that satisfies (19b) since $\hat{A}_{\mathcal{N}\mathcal{N}}$ is Schur $\rho\big(\hat{A}_{\mathcal{N}\mathcal{N}}\big) < 1$. By (16), the Lyapunov equation (19a) holds in the nominal configuration $\varsigma = \mathbf{1}$. We will uses this fact to show that (19a) holds in general. Note that $\begin{bmatrix} \hat{P}_{\mathcal{A}} & 0 \\ 0 & 0 \end{bmatrix} \preceq \begin{bmatrix} \hat{P}_{\mathcal{A}} & 0 \\ 0 & \hat{P}_{\mathcal{N}} \end{bmatrix}$ for any partitions $(\mathcal{A}, \mathcal{N})$ of active $\mathcal{A}$ and inactive $\mathcal{N}$ units. Thus by (16) we have

$$\begin{aligned} &\begin{bmatrix} \bar{A}_{\mathcal{A}\mathcal{A}} & \bar{A}_{\mathcal{A}\mathcal{N}} \\ \bar{A}_{\mathcal{N}\mathcal{A}} & \bar{A}_{\mathcal{N}\mathcal{N}} \end{bmatrix}' \begin{bmatrix} \hat{P}_{\mathcal{A}} & 0 \\ 0 & 0 \end{bmatrix} \begin{bmatrix} \bar{A}_{\mathcal{A}\mathcal{A}} & \bar{A}_{\mathcal{A}\mathcal{N}} \\ \bar{A}_{\mathcal{N}\mathcal{A}} & \bar{A}_{\mathcal{N}\mathcal{N}} \end{bmatrix} - \begin{bmatrix} \hat{P}_{\mathcal{A}} & 0 \\ 0 & \hat{P}_{\mathcal{N}} \end{bmatrix} \quad (20) \\ &\quad \preceq \begin{bmatrix} \bar{A}_{\mathcal{A}\mathcal{A}} & \bar{A}_{\mathcal{A}\mathcal{N}} \\ \bar{A}_{\mathcal{N}\mathcal{A}} & \bar{A}_{\mathcal{N}\mathcal{N}} \end{bmatrix}' \begin{bmatrix} \hat{P}_{\mathcal{A}} & 0 \\ 0 & \hat{P}_{\mathcal{N}} \end{bmatrix} \begin{bmatrix} \bar{A}_{\mathcal{A}\mathcal{A}} & \bar{A}_{\mathcal{A}\mathcal{N}} \\ \bar{A}_{\mathcal{N}\mathcal{A}} & \bar{A}_{\mathcal{N}\mathcal{N}} \end{bmatrix} - \begin{bmatrix} \hat{P}_{\mathcal{A}} & 0 \\ 0 & \hat{P}_{\mathcal{N}} \end{bmatrix} \\ &\quad \preceq \begin{bmatrix} -\hat{C}'_{\mathcal{A}\mathcal{A}}\hat{Q}_{\mathcal{A}}\hat{C}_{\mathcal{A}\mathcal{A}} - \hat{K}'_{\mathcal{A}\mathcal{A}}\hat{R}_{\mathcal{A}}\hat{K}_{\mathcal{A}\mathcal{A}} & * \\ * & * \end{bmatrix} \end{aligned}$$

where $*$ denotes irrelevant terms and the closed-loop dynamics $\bar{A}$ matrix is given by

$$\bar{A} = \begin{bmatrix} \bar{A}_{\mathcal{A}\mathcal{A}} & \bar{A}_{\mathcal{A}\mathcal{N}} \\ \bar{A}_{\mathcal{N}\mathcal{A}} & \bar{A}_{\mathcal{N}\mathcal{N}} \end{bmatrix} = \begin{bmatrix} \hat{A}_{\mathcal{A}\mathcal{A}} + \hat{B}_{\mathcal{A}\mathcal{A}}\hat{K}_{\mathcal{A}\mathcal{A}} & * \\ * & * \end{bmatrix}$$

Pre- and post-multiplying (20) by $\left[\begin{smallmatrix} I & 0 \\ 0 & 0 \end{smallmatrix}\right]$ produces the Lyapunov inequality

$$\begin{aligned} (\hat{A}_{\mathcal{A}\mathcal{A}} + \hat{B}_{\mathcal{A}\mathcal{A}}\hat{K}_{\mathcal{A}\mathcal{A}})'\hat{P}_{\mathcal{A}}(\hat{A}_{\mathcal{A}\mathcal{A}} + \hat{B}_{\mathcal{A}\mathcal{A}}\hat{K}_{\mathcal{A}\mathcal{A}}) - \hat{P}_{\mathcal{A}} \quad (21) \\ \preceq -\hat{C}'_{\mathcal{A}\mathcal{A}}\hat{Q}_{\mathcal{A}}\hat{C}_{\mathcal{A}\mathcal{A}} - \hat{K}'_{\mathcal{A}\mathcal{A}}\hat{R}_{\mathcal{A}}\hat{K}_{\mathcal{A}\mathcal{A}}. \end{aligned}$$

Thus the Lyapunov inequality (19a) holds since $\hat{Q}_{\mathcal{A}} \succ 0$ and the pair $(\hat{A}_{\mathcal{A}\mathcal{A}}, \hat{C}_{\mathcal{A}\mathcal{A}})$ is observable by Proposition III.1. Therefore the closed-loop system (18) is asymptotically stable and the offset states $\tilde{x} \to 0$ converge to zero. □

We call the configuration-dependent linear controller (13) a *reconfigurable linear controller* since it stabilizes the system (7) in any configuration ς. In the next section we will use the reconfigurable linear controller (13) to design a reconfigurable model predictive controller that achieves the constraint satisfaction control objective in addition to the tracking objective.

The design of a controller gain (14) and Lyapunov matrix (15) that satisfy the discrete-time Lyapunov equation (16) can be posed as the following linear matrix inequality using standard techniques (see, e.g., [21, Sec. 3.4], [14])

$$\begin{bmatrix} X & * & * & * \\ \hat{A}^{\mathbf{1}}X + \hat{B}^{\mathbf{1}}Y & X & * & * \\ (\hat{Q}^{\mathbf{1}})^{1/2}\hat{C}^{\mathbf{1}}X & 0 & I & * \\ (\hat{R}^{\mathbf{1}})^{1/2}Y & 0 & 0 & I \end{bmatrix} \succeq 0 \quad (22)$$

where the $\hat{P}^{\mathbf{1}} = X^{-1}$ is the Lyapunov matrix and $\hat{K}^{\mathbf{1}} = YX^{-1}$ is the controller gain. In general, the linear matrix inequality (22) may not be feasible in which case the hypothesis of Lemma III.2 will not hold. For the purposes of this paper, we assume that (22) has a solution. In general, the existence of a solution can be guaranteed if the matrix $\hat{B}^{\mathbf{1}}$ is block diagonal or block upper-triangular [22].

D. Reconfigurable Model Predictive Controller

In this section we present a reconfigurable model predictive controller for the ME-VCS that achieves the tracking objective while satisfying input and state constraints.

First we examine when it is possible to satisfy the constraints (2). The state constraint set for the composite augmented state $\hat{x} = \operatorname{col}(\hat{x}_0, \hat{x}_1, \ldots, \hat{x}_N)$ is given by

$$\hat{\mathcal{X}}(w_0) = \big(\mathcal{X}_0(w_0) \times \mathcal{U}_0\big) \times \Big(\textstyle\prod_{i=1}^{N} \mathbb{R}^{n_i} \times \mathcal{U}_i \times \mathbb{R}\Big). \quad (23)$$

The set $\hat{\mathcal{X}}(w_0)$ does not depend on the configuration ς. However it may not be possible to satisfy the constraints $\hat{x}(t) \in \hat{\mathcal{X}}$ for every configuration ς since the state $x_0(t)$ of the outdoor unit $i = 0$ depends (3a) on the inputs $u_j(t)$ for all the indoor units $j = 1, \ldots, N$. Thus, when units are inactive $\varsigma_j = 0$, we have less control authority over the outdoor unit state $x_0(t)$. We define the following configuration-dependent maximal control invariant set

$$\begin{aligned} \hat{\mathcal{C}}^{\varsigma}_{\infty}(w, r) = \Big\{ \hat{x} \in \hat{\mathcal{X}}(w_0) : \exists \Delta u \in \Delta\mathcal{U} \text{ s.t.} \quad (24) \\ \hat{A}^{\varsigma}\hat{x} + \hat{B}^{\varsigma}\Delta u + \hat{B}^{\varsigma}_{r} r + \hat{B}^{\varsigma}_{w} w \in \hat{\mathcal{C}}^{\varsigma}_{\infty}(w, r) \Big\}. \end{aligned}$$

The volume of the control invariant $\hat{\mathcal{C}}^{\varsigma}_{\infty}(w, r)$ changes depending on the configuration ς. However the control invariant set (24) is always non-empty $\hat{\mathcal{C}}^{\varsigma}_{\infty}(0, 0) \neq \varnothing$ and contains the origin in its interior $0 \in \operatorname{int}\big(\hat{\mathcal{C}}^{\varsigma}_{\infty}(0, 0)\big)$ for any configuration ς since the pair $(\hat{A}_{\mathcal{A}\mathcal{A}}, \hat{B}_{\mathcal{A}\mathcal{A}})$ is controllable, the matrix $\hat{A}_{\mathcal{N}\mathcal{N}}$ is Schur, and the sets $\hat{\mathcal{X}}(0)$ and $\Delta\mathcal{U}$ contain the origin in their interiors. Furthermore the set $\hat{\mathcal{C}}^{\varsigma}_{\infty}(w, r)$ is non-empty and contains the desired equilibrium state $\hat{x}^{\infty}$ in its interior for sufficiently small disturbances w and references r. The stability and constraint satisfaction results will only hold on subsets of the invariant set (24).

The reconfigurable model predictive controller computes the control input by solving the following constrained finite-time optimal control problem

$$\min_{\Delta\mathbf{u}} \sum_{i=0}^{N}\Big(\varsigma_i\|\hat{x}_{i,T|t}-\hat{x}_i^{\infty}\|^2_{\hat{P}_i}+ +\sum_{k=0}^{T-1}\varsigma_i\|\hat{z}_{i,k|t}\|^2_{\hat{Q}_i^z}+\phi_i\|\Delta u_{i,k|t}\|^2_{\hat{R}_i}\Big) \quad (25a)$$

$$\text{s.t. } u_{i,k|t}\in\mathcal{U}_i,\ \Delta u_{i,k|t}\in\Delta\mathcal{U}_i,\ x_{0,k+1|t}\in\mathcal{X}_0 \quad (25b)$$

$$\begin{aligned}\hat{x}_{k+1|t}&=\hat{A}^{\mathbf{1}}\hat{x}_{k|t}+\hat{B}^{\mathbf{1}}\Delta u_{k|t}+\hat{B}_r^{\mathbf{1}}r_{k|t}+\hat{B}_w^{\mathbf{1}}w_{k|t}\\ r_{k+1|t}&=r_{k|t}+\hat{E}\Delta u_{k|t}\\ w_{k+1|t}&=w_{k|t}\\ \hat{z}_{k|t}&=\hat{C}_z\hat{x}_{k|t}+\hat{D}_r r_{k|t}+\hat{D}_r r_{k|t}\end{aligned} \quad (25c)$$

$$\begin{aligned}x_{0|t}&=x(t),u_{-1|t}=\varsigma_i u(t-1),\\ r_{0|t}&=r(t),w_{0|t}=w(t)\end{aligned} \quad (25d)$$

where $\hat{x}_{k|t}$ is the predicted augmented state under the incremental input $\Delta u_{k|t}$ over the horizon T, and $\Delta\mathbf{u}=\mathrm{col}(\Delta u_{0,0|t},\dots,\Delta u_{N,0|t},\dots,\Delta u_{N,T-1|t},\dots,\Delta u_{N,T-1|t})$ is the optimization variable. The reconfigurable model predictive controller integrates the optimal incremental input $\Delta u^{\star}_{i,k|t}$ to obtain the implemented input

$$u_i(t)=\varsigma_i u_i(t-1)+\Delta u^{\star}_{i,0|t} \quad (26)$$

for each unit $i=0,\dots,N$.

The cost function (25a) of the constrained finite-time optimal control problem (25) is configuration-dependent. The term $\varsigma_i\|\hat{z}_{i,k|t}\|^2_{\hat{Q}_i^z}$ penalizes the performance outputs of the augmented model (7). For the outdoor unit $i=0$, the performance output $\hat{z}_0=z_0-r_0$ is the difference between the discharge temperature $z_0=\mathrm{Td}$ and the reference discharge temperature $r_0=\mathrm{Td}_{\mathrm{ref}}$, which maximizes energy efficiency. Since the outdoor unit is always active $\varsigma_0=1$, the model predictive control always regulates the discharge temperature. For the indoor units $i=1,\dots,N$, the performance outputs $\hat{z}_i=\mathrm{col}(z_i-r_i,\xi)$ includes the room temperature tracking errors z_i-r_i, and their integrals ξ. If an indoor unit is inactive $\varsigma_i=0$, then the room temperature tracking error and integrated error for that indoor unit do not appear in the cost $\varsigma_i\|\hat{z}_{i,k|t}\|^2_{\hat{Q}_i^z}=0$. Thus, the reconfigurable MPC does not regulate the room temperature of inactive zones.

The term $\phi_i\|\Delta u_{i,k|t}\|^2_{\hat{R}_i}$ in the cost function (25a) penalizes changes $\Delta u_{i,k|t}$ to the inputs $u_{i,k|t}$. For the outdoor unit $i=0$, this term penalizes changing the compressor frequency and outdoor fan speed. For the indoor units $i=1,\dots,N$ this term penalizes changing in cooling capacity command. The scalar ϕ_i is defined as

$$\phi_i=\begin{cases}1 & \text{if } \varsigma_i=1\\ M & \text{if } \varsigma_i=0\end{cases} \quad (27)$$

where the "big-M" scalar M is chosen to be large compared to the eigenvalues of the matrices $\hat{Q}_i$, $\hat{R}_i$, and $\hat{P}_i$. The scalar ϕ_i ensures the optimal incremental input $\Delta u^{\star}_{i,k|t}=0$ is zero for inactive indoor units $\varsigma_i=0$ [23]. Thus, the cooling capacity command $u_{i,k|t}=u_{i,k-1|t}+\Delta u_{i,k|t}=0$ to an inactive room $\varsigma_i=0$ is zero since it is initially zero $u_{i,-1|t}=\varsigma_i u_i(t-1)$ and does not change $\Delta u_{i,k|t}=0$ for $k=0,\dots,T-1$.

The terminal cost term $\varsigma_i\|\hat{x}_{i,T|t}-\hat{x}_i^{\infty}\|^2_{\hat{P}_i}$ penalizes the deviation of the augmented state $\hat{x}_{i,N|t}$ from the desired terminal equilibrium $\hat{x}_i^{\infty}$ for $i=0,\dots,N$. When the i-th indoor unit is inactive $\varsigma_i=0$, its terminal cost is zero $\varsigma_i\|\hat{x}_{i,T|t}-\hat{x}_i^{\infty}\|^2_{\hat{P}_i}=0$. The terminal cost matrices $\hat{P}_i$ are the Lyapunov matrices (15) for the linear controller (13) and satisfy (16). We will show that this terminal cost guarantees the stability of the model predictive controller (26) in closed-loop with the augmented system (7).

The prediction model (25c) used by the model predictive controller does not depend on the configuration ς of the ME-VCS. Instead the optimal control problem (25) uses the model (25c) for the nominal configuration $\varsigma=\mathbf{1}$. The following lemma shows that, due to the structure of the cost (25a), solving the optimal control problem (25) with the configuration-independent prediction model (25c) is equivalent to solving the problem with the correct configuration-dependent model (7).

Lemma III.3. *Let $\hat{x}(t)\in\hat{\mathcal{C}}^{\varsigma}_{\infty}(w,r)\neq\varnothing$. Let $u^{\star}_{i,k|t}$ and $\Delta u^{\star}_{i,k|t}$ be the optimal solution to problem* (25) *and let $u^{\varsigma}_{i,k|t}$ and $\Delta u^{\varsigma}_{i,k|t}$ be the solution when the model* (25c) *is configuration ς dependent. Then $u^{\star}_{i,k|t}=u^{\varsigma}_{i,k|t}$ and $\Delta u^{\star}_{i,k|t}=\Delta u^{\varsigma}_{i,k|t}$.*

Proof. We will show that replacing the configuration-independent prediction model (25c) with the configuration-dependent model (7), does not change the solution to the optimal control problem (25).

If an indoor unit is inactive $\varsigma_i=0$ then the initial input $u_{i,-1|t}=\varsigma_i u(t-1)=0$ is set to zero and the cost $\phi_i\|\Delta u_{i,k|t}\|^2_{\hat{R}_i}$ of changing the input is effectively infinite since $\phi_i=M\gg\bar{\lambda}_P,\bar{\lambda}_Q,\bar{\lambda}_R$. Thus, the optimal control problem (25) will not change the input $\Delta u_{i,k|t}=0$ for $\varsigma_i=0$ if this is a feasible solution. This choice $\Delta u_{i,k|t}=0$ satisfies the input $u_{i,k|t}=u_{i,k-1|t}+\Delta u_{i,k|t}=0\in\mathcal{U}_i$ and incremental input $\Delta u_{i,k|t}=0\in\Delta\mathcal{U}_i$ constraints since the sets $\mathcal{U}_i$ and $\Delta\mathcal{U}_i$ contain the origin. Furthermore, since $\hat{x}(t)\in\hat{\mathcal{C}}^{\varsigma}_{\infty}(w,r)$ there exists feasible incremental inputs $\Delta u_{i,k|t}$ for only the active units $i\in\mathcal{A}$ such that the augmented state constraints $\hat{\mathcal{X}}(w_0)$ can be satisfied since

$$\hat{A}^{\varsigma}\hat{x}+\hat{B}^{\varsigma}\Delta u+\hat{B}^{\varsigma}_r r+\hat{B}^{\varsigma}_w w\in\hat{\mathcal{C}}^{\varsigma}_{\infty}(w,r)$$

and $\hat{\mathcal{C}}^{\varsigma}_{\infty}(w,r)\subseteq\hat{\mathcal{X}}(w_0)$. Thus the optimal input and incremental input sequences produced by the optimal control problem (25) satisfies

$$\Delta u^{\star}_{i,k|t}=\varsigma_i\Delta u^{\star}_{i,k|t} \quad (28a)$$

$$u^{\star}_{i,k|t}=\varsigma_i u^{\star}_{i,k|t} \quad (28b)$$

for each $i=0,\dots,N$. Plugging the configuration-dependent inputs (28) into the configuration-independent prediction model (25c) produces the configuration-dependent model

$$\begin{bmatrix}\hat{x}_{\mathcal{A}}(t+1)\\ \hat{x}_{\mathcal{N}}(t+1)\end{bmatrix}=\begin{bmatrix}\hat{A}_{\mathcal{A}\mathcal{A}} & 0\\ \hat{A}_{\mathcal{N}\mathcal{A}} & \hat{A}^{\mathbf{1}}_{\mathcal{N}\mathcal{N}}\end{bmatrix}\begin{bmatrix}\hat{x}_{\mathcal{A}}(t)\\ \hat{x}_{\mathcal{N}}(t)\end{bmatrix}+\begin{bmatrix}\hat{B}_{\mathcal{A}\mathcal{A}} & 0\\ \hat{B}_{\mathcal{N}\mathcal{A}} & 0\end{bmatrix}\begin{bmatrix}\Delta u_{\mathcal{A}}(t)\\ \Delta u_{\mathcal{N}}(t)\end{bmatrix} + \begin{bmatrix}\hat{B}_{r,\mathcal{A}\mathcal{A}} & 0\\ \hat{B}_{r,\mathcal{N}\mathcal{A}} & 0\end{bmatrix}\begin{bmatrix}r_{\mathcal{A}}(t)\\ r_{\mathcal{N}}(t)\end{bmatrix}+\begin{bmatrix}\hat{B}_{w,\mathcal{A}\mathcal{A}} & 0\\ \hat{B}_{w,\mathcal{N}\mathcal{A}} & 0\end{bmatrix}\begin{bmatrix}w_{\mathcal{A}}(t)\\ w_{\mathcal{N}}(t)\end{bmatrix}.$$

This model incorrectly predicts the states $\hat{x}_{\mathcal{N}}$ of the inactive units $\mathcal{N}=\{i\in\mathcal{I}:\varsigma_i=0\}$. However, by Proposition III.1 these states are not observable in the cost function (25a) since $\varsigma_i\|\hat{z}_{i,k|t}\|^2_{\hat{Q}_i^z}=0$ when $\varsigma_i=0$. In addition, these incorrectly

predicted states $\hat{x}_{\mathcal{N}}$ do not affect the constraints (25b) of the optimal control problem (25) since the ME-VCS only has state constraints on the outdoor unit which is always active $0 \in \mathcal{A}$. Thus, the incorrect sub-model for the inactive states $\hat{x}_{\mathcal{N}}$ can be ignored since it does not affect the cost or feasible region of the optimal control problem. On the other hand, this model correctly predicts the states $\hat{x}_{\mathcal{A}}$ of the active units $\mathcal{A} = \{i \in \mathcal{I} : \varsigma_i = 1\}$ since the state $\hat{x}_{\mathcal{N}}$ of the inactive units do not affect the active units. Thus, the relevant portion of the model is correct and therefore the optimal control problem (25) yields the same solution as if the correct model (7) was used. □

Lemma III.3 means that we can prove theoretical results about the model predictive controller (26) under the assumption that the optimal control problem (25) is configuration-dependent without having to change the prediction model (25c) in practice. In particular, the following theorem shows that the model predictive controller (26) stabilizes the augmented system (7).

Theorem III.4. *Let* (14) *and* (15) *satisfy* (16). *Let* $\hat{\mathcal{C}}^{\varsigma}_{\infty}(w,r) \neq \varnothing$ *be non-empty. Consider the model predictive controller* (26) *in closed-loop with the configuration-dependent augmented system* (7). *Then there exists a non-empty domain* $\mathcal{O} \neq \varnothing$ *such that for all* $x(0) \in \mathcal{O} \subseteq \hat{\mathcal{C}}^{\varsigma}_{\infty}(w,r)$ *we have*

1) *The closed-loop state* $x_0(t) \to x_0^{\infty}$ *and input* $u_0(t) \to u_0^{\infty}$ *of the outdoor unit* $i = 0$ *converge to their desired equilibrium values* x_0^{∞} *and* u_0^{∞}, *respectively. The discharge temperature* $z_0(t) \to r_0^{\infty}$ *converges to its desired reference value* r_0^{∞}.
2) *The closed-loop states* $x_i(t) \to x_i^{\infty}$ *and inputs* $u_i(t) \to u_i^{\infty}$ *for the active indoor units* $\varsigma_i = 1$ *converge to their desired equilibrium values* x_i^{∞} *and* u_i^{∞}, *respectively. The room temperatures* $z_i(t) \to r_i^{\infty}$ *converge to their reference values* r_i^{∞}.
3) *The closed-loop states* $x_i(t)$ *of the inactive indoor units* $\varsigma_i = 0$ *converge to zero. The room temperatures* $z_i(t) \to D_{w,ii} w_i^{\infty}$ *are bounded and converge to some steady-state temperatures* $D_{w,ii} w_i^{\infty}$ *which depend on the constant heat loads* w_i^{∞}.
4) *The closed-loop state* $x_0(t)$ *and input* $u_0(t)$ *for the outdoor unit satisfy the constraints* (2).
5) *The closed-loop states* $x_i(t)$ *and inputs* $u_i(t)$ *for the active indoor units* $\varsigma_i = 1$ *satisfy the constraints* (2).
6) *The closed-loop states* $x_i(t)$ *and inputs* $u_i(t)$ *for the inactive indoor units* $\varsigma_i = 0$ *satisfy the constraints* (2).

Proof. According to Proposition III.1, the augmented system (7) has the structure

$$\begin{bmatrix} \tilde{x}_{\mathcal{A}}(t+1) \\ \tilde{x}_{\mathcal{N}}(t+1) \end{bmatrix} = \begin{bmatrix} \hat{A}_{\mathcal{A}\mathcal{A}} & 0 \\ 0 & \hat{A}_{\mathcal{N}\mathcal{N}} \end{bmatrix} \begin{bmatrix} \tilde{x}_{\mathcal{A}}(t) \\ \tilde{x}_{\mathcal{N}}(t) \end{bmatrix} + \begin{bmatrix} \hat{B}_{\mathcal{A}\mathcal{A}} 0 \\ 0 \; 0 \end{bmatrix} \begin{bmatrix} \Delta u_{\mathcal{A}}(t) \\ \Delta u_{\mathcal{N}}(t) \end{bmatrix}$$

where $\tilde{x}_{\mathcal{A}} = \hat{x}_{\mathcal{A}} - \hat{x}^{\infty}_{\mathcal{A}}$ and $\tilde{x}_{\mathcal{N}} = \hat{x}_{\mathcal{N}}$ are the augmented offset states. The dynamics of the active $\tilde{x}_{\mathcal{A}}$ and inactive $\tilde{x}_{\mathcal{N}}$ states are decoupled. By Proposition III.1 the inactive dynamics are stable. Thus claim 3 holds. The inputs $u_i(t) = 0 \in \mathcal{U}_i$ and increment inputs $u_i(t) - u_i(t-1) = 0 \in \Delta\mathcal{U}_i$ to the inactive indoor units $\varsigma_i = 0$ satisfy the constraints (2c) and (2e) since the sets $\mathcal{U}_i$ and $\Delta\mathcal{U}_i$ contain the origin. Furthermore there are no constraints on the states of the indoor units. Thus claim 6 holds.

The model predictive controller (26) is used to stabilize the active dynamics

$$\tilde{x}_{\mathcal{A}}(t+1) = \hat{A}_{\mathcal{A}\mathcal{A}} \tilde{x}_{\mathcal{A}}(t) + \hat{B}_{\mathcal{A}\mathcal{A}} \Delta u^{\star}_{\mathcal{A},0|t}. \tag{29}$$

As shown in Lemma III.3, the optimal control problem (25) uses the correct model (29). Thus we can prove that the model predictive controller (26) stabilizes the active subsystem (29) using the standard approach, where the optimal value function (25a) is used as a Lyapunov function $V(x) = J^{\star}(x)$. We will use the linear controller (13) to show that the Lyapunov function $V(x)$ decreases on some non-empty set $\mathcal{O}$.

The desired equilibrium state $x_i^{\infty} \in \operatorname{int}(\mathcal{X}_i)$ and input $u_i^{\infty} \in \operatorname{int}(\mathcal{U}_i)$ are contained in the interiors of the sets $\mathcal{X}_i$ and $\mathcal{U}_i$ respectively for $i = 0, \ldots, N$. Thus, the set $\hat{\mathcal{C}}^{\varsigma}_{\infty}(w,r)$ is non-empty and $\hat{\mathcal{C}}^{\varsigma}_{\infty}(w,r) - \hat{x}^{\infty}$ contains the origin in its interior. Thus, the system (29) in closed-loop with the controller $\Delta u = \hat{K}^{\varsigma}_{\mathcal{A}\mathcal{A}} \tilde{x}_{\mathcal{A}}$ has a non-empty positive invariant set $\mathcal{O}_1 \neq \varnothing$ since the closed-loop system is stable and the sets $\Delta\mathcal{U}$ and $\hat{\mathcal{C}}^{\varsigma}_{\infty}(w,r) - \hat{x}^{\infty}$ contain neighborhoods of the origin. Since the linear controller (13) satisfies (21) we can conclude that the value function (25) decreases in closed-loop for states $\hat{x}(t) \in \mathcal{O}_2$ in some larger set $\mathcal{O}_2 \supseteq \mathcal{O}_1 \neq \varnothing$. Thus claims 1 and 2 hold on the non-empty domain $\mathcal{O}_2$.

Finally we note that since the model predictive controller (26) stabilizes the augmented system (7) in a neighborhood $\mathcal{O}_2$ of the desired equilibrium $\hat{x}^{\infty}$, there exists a non-empty-interior positive invariant $\mathcal{O} \subseteq \mathcal{O}_2$ for which the closed-loop states $\hat{x}(t)$ and inputs $\Delta u(t)$ satisfy the constraints (2) since $\hat{\mathcal{C}}^{\varsigma}_{\infty}(w,r) - \hat{x}^{\infty} \subseteq \hat{\mathcal{X}}(w_0) - \hat{x}^{\infty}$ and $\Delta\mathcal{U}$ contain the origin in their interiors. Thus claims 4 and 5 hold on such non-empty-interior domain $\mathcal{O}$. □

In practice, the ME-VCS can switch configurations $\varsigma(t) \neq \varsigma(t+1)$, but the switches are infrequent compared to the timescale of the model (3). It is well known that if each configuration is stable and the system dwells in each configuration for a sufficiently long time, then the switched system is stable [22]. This result was recently extended to system stabilized by model predictive controllers [24]. Therefore we conclude that the reconfigurable model predictive controller (26) stabilizes the configuration-dependent ME-VCS (7) when there is sufficient time between changes in the configuration ς. This fact will be verified in our simulation and experimental results in the next section.

IV. Validation and Comparison

In this section, simulations and experimental results are presented that validate the reconfigurable MPC approach. Section IV-A describes the experimental facility used to demonstrate the performance of the reconfigurable MPC on a two-zone vapor compression system. Linearized models are obtained from the experimental system and these models are used to design the reconfigurable MPC. In IV-B the reconfigurable MPC is compared to a collection of independently designed model predictive controllers for each configuration in simulations, that are further validated with experiments.

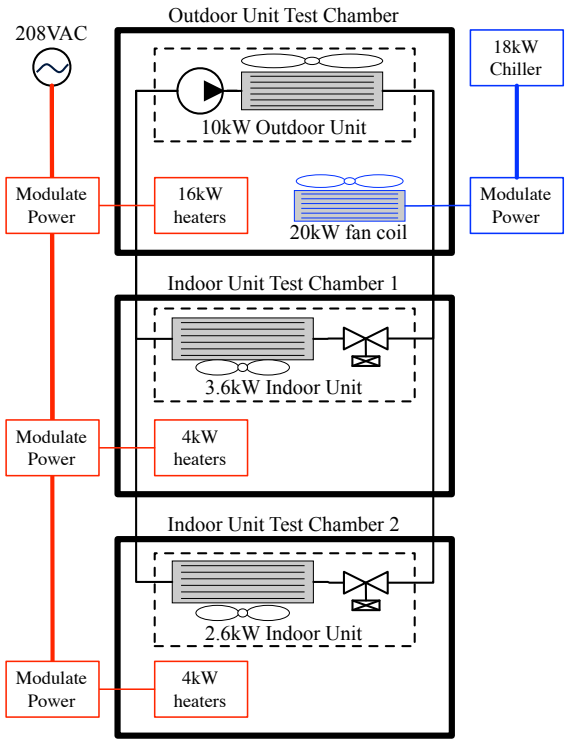

Fig. 2. The outdoor unit and two indoor units of a split-ductless style vapor compression system is installed in three test chambers. A balance-of-plant system consists of a set of adjustable-power heaters (red) and an adjustable-power hydronic system (blue), and is used to manage the boundary conditions of the vapor compression system under test.

A. Experimental Facility

A two-zone commercially-available vapor compression system, and a supporting HVAC system necessary for generating loads and regulating boundary conditions are installed in a test facility as shown schematically in Fig. 2. The ME-VCS outdoor unit (consisting of the compressor, condensing heat exchanger and associated fan) is installed in a 6.3 m^3 insulated test chamber and is connected via refrigerant lines to two indoor units, which are installed in separate 9.9 m^3 insulated test chambers. The boundary conditions for this system are the heat loads injected in the indoor unit test chambers and the air temperature in the outdoor unit test chamber.

In addition to the vapor compression system, the experimental facility also includes a balance-of-plant system consisting of variable power heaters and variable power chilled water fan coils and associated controllers configured to regulate the heat loads in the indoor unit test chambers and the air temperature in the outdoor unit test chamber.

The plant model used in the following simulation and model predictive controller is derived from experimental data collected in this test facility. With 1.6 kW fixed heat loads applied in the indoor unit test chambers, the outdoor test chamber regulated to 35°C, and the vapor compression system operating at steady state, steps are separately applied to each control input u (CF, ODF, CCC_1 and CCC_2). Measurements of the system outputs y (Td, Te, Tc, Tr_1 and Tr_2) are collected and a state space model of the plant in the form of Equation (1) is obtained. The conditions of the operating point about which the linear model is created are summarized in Table II.

TABLE II
OPERATING POINT OF THE VCS SELECTED FOR LINEARIZATION.

Inputs, u		**Outputs,** y		**Boundary Conditions,** w	
compressor freq (CF)	28 Hz	discharge temp (Td)	63°C		
outdoor fan speed (ODF)	525 rpm	condensing temp (Tc)	40°C	outdoor air temp (OAT)	35°C
cooling cap cmd 1 (CCC_1)	65%	zone temp 1 (Tr_1)	27°C	heat load 1 (Q_1)	1.6 kW
cooling cap cmd 2 (CCC_2)	65%	zone temp 2 (Tr_2)	24°C	heat load 2 (Q_2)	1.6 kW

B. Reconfigurable MPC vs. a Collection of Controllers

The main advantage of reconfigurable MPC is the reduction in the number of parameters that specify controllers for all configurations of a ME-VCS while preserving transient performance. We demonstrate this by comparing the tuning effort and memory storage requirements of reconfigurable MPC to a collection of model predictive controllers where each is designed for a single configuration.

Commercial multi-evaporator air conditioners can be configured with 50 or more evaporators. Designing model predictive controllers for all possible configurations would require 2^{50} individual controllers. In addition, it would require an unrealistically large amount of memory to store the associated controller parameters. In contrast, the memory required for a 50-zone reconfigurable MPC design is approximately 3.4 MB, which compares favorably to the few megabytes of memory typically available for embedded microcontrollers [20]. Table III compares the reconfigurable MPC approach with a set of independently-designed model predictive controllers in terms of (i) the number of elements in the system matrices (SM) required to specify the optimal control problem for all configurations, (ii) the number of elements in the penalty matrices (PM) that must be tuned and (iii) the associated memory requirements (MR) to store the controller parameters assuming double precision representation. The table shows that design effort and memory requirements for the reconfigurable MPC grow linearly with the number of zones instead of exponentially as in the case of the collection of controllers.

TABLE III
COMPARISON OF SYSTEM MATRICES (SM), PENALTY MATRICES (PM), AND MEMORY REQUIRED (MR) BETWEEN A SET OF MPC CONTROLLERS AND THE RECONFIGURABLE MPC APPROACH.

NO. of Zones	Elements in SM and PM and Megabytes of MR to store controller parameters					
	Set of MPC Controllers			Reconfigurable MPC		
	(SM)	(PM)	(MR) MB	(SM)	(PM)	(MR) MB
2	3.5e3	2.5e3	0.092	880	613	0.023
8	1.25e6	9.25e5	33.3	4.9e3	3.6e3	0.13
50	1.4e20	1.1e20	3.8e15	1.24e5	9.5e4	3.4

Next we compare the transient performance of the reconfigurable MPC and the collection of individual controllers observed during simulations.

The proposed reconfigurable MPC is designed according to the approach outlined in Section III. Model augmentations are applied as described, creating the configuration-dependent

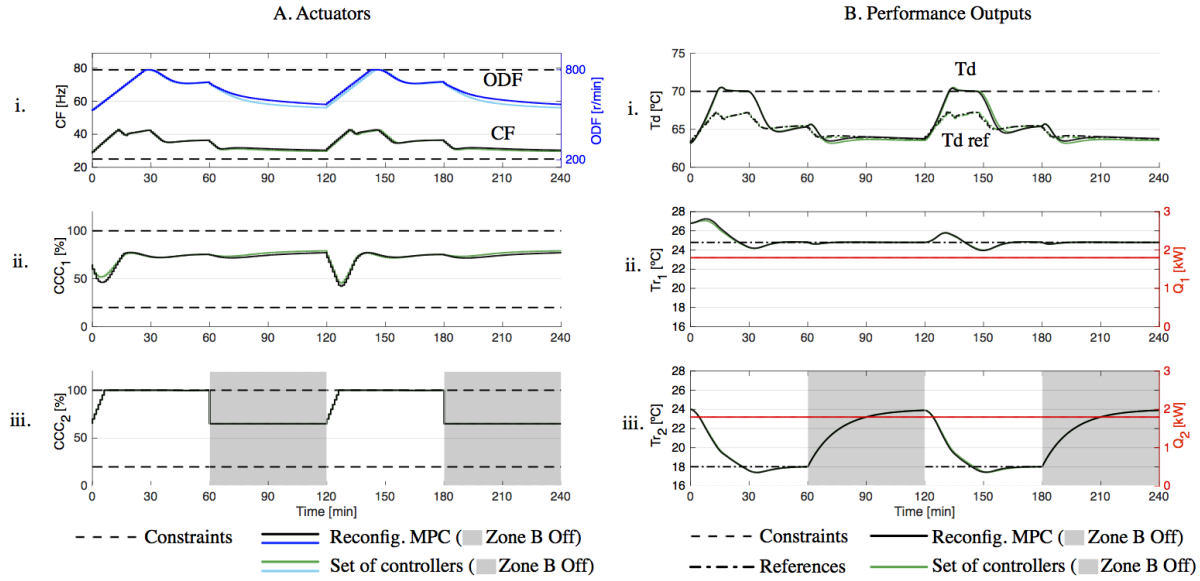

Fig. 3. Simulation of a two-zone multi-evaporator VCS where zone 2 is periodically switched off (when the zone is off, the plots are shaded gray). Performance of the proposed reconfigurable MPC method is compared to a set of independently-designed controllers. The closed loop performance is shown to be largely similar, however, the number of system matrices stored in memory and the design/tuning parameters required for the reconfigurable method are substantially fewer. The actuators are shown on the left (A) and the performance outputs are shown on the right (B). The performance outputs most strongly associated with a particular actuator are plotted on the same row (*i.e.*, compressor frequency with compressor discharge temp., and cooling command for zone 1 with the air temp. in that zone.)

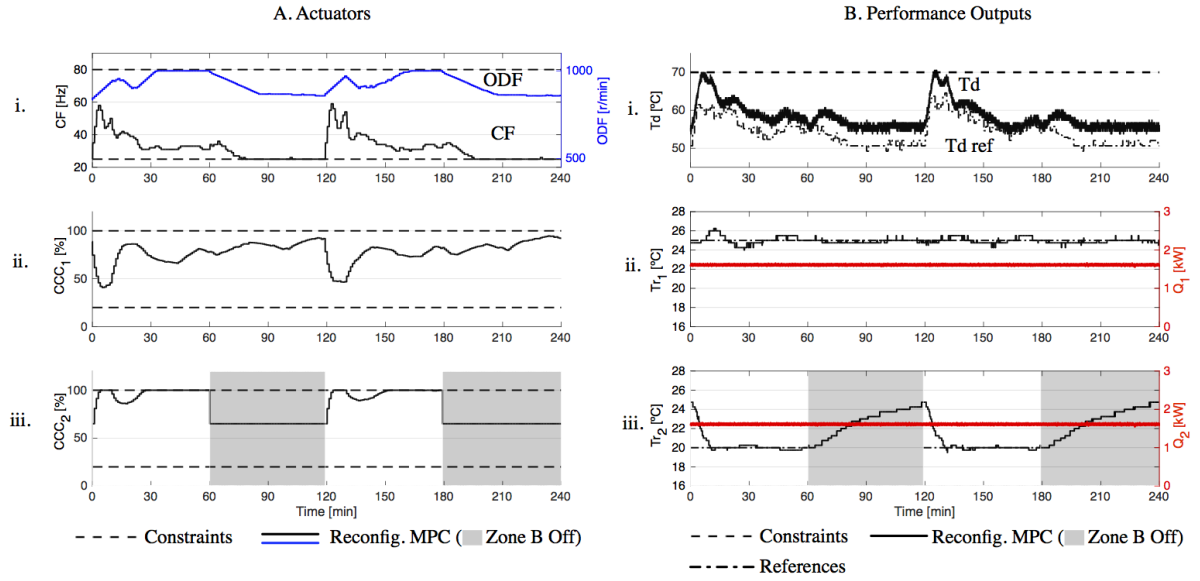

Fig. 4. Experiment largely reproducing the conditions tested in simulation in Fig. 3. The reconfigurable MPC controlling a production ME-VCS in a laboratory setting is shown to perform similarly to simulations of the linearized plant. (The method of designing a set of MPC controllers is not implemented in experiments).

model (7), and a reconfigurable model predictive controller is designed to achieve the tracking objective while satisfying constraints. At runtime, the configuration ς of the ME-VCS is determined and a controller is synthesized from the configuration-dependent optimal control problem (25).

For comparison, a collection of two independently-designed and tuned MPC controllers is created following the traditional approach—one for a single evaporator turned on and another for two evaporators turned on. The two controllers are designed offline and stored, and the appropriate controller is loaded from memory at runtime. The reference tracking and constraint enforcement performance of both methods is compared for a two-zone multi-evaporator vapor compression system undergoing reconfiguration where one zone is periodically switched on and off.

In the following simulations and experiments, and for both the reconfigurable MPC and the collection of individual controllers, the sampling period of the controller is 1 minute and the prediction horizon is 16 minutes. For both controllers the optimal control problem is converted into a quadratic program and solved with the solver in [25].

The simulation results are shown in Fig. 3, in which Fig. 3A shows the actuator values: (i) CF and ODF, (ii) CCC_1, and (iii) CCC_2. Fig. 3B shows the performance outputs and some of

the constrained outputs: (i) Td and Td_{ref}, (ii) Tr_1, $\text{Tr}_{1,\text{ref}}$ and Q_1, (iii) Tr_2, $\text{Tr}_{2,\text{ref}}$ and Q_2. Te and Tc temperatures are also constrained outputs, but these constraints were not active and therefore have been omitted from the plots for clarity.

After the initial transient with both zones turned on, zone 2 is switched off at 60 minutes. With zone 2 switched off, the actuator associated with that zone (CCC_2, Fig. 3A-iii) is reset to the equilibrium of the linearized model (CCC_2 is set to the origin in linearized coordinates, or 65% in engineering units as shown in Table II). Since this actuator setting provides a cooling capacity that is too low to meet the heat load, the air temperature in that zone increases (Fig. 3B-iii). When the zone is switched on, the air is warmer than the 18°C setpoint, so CCC_2 is increased to its maximum value ($\text{CCC}_{2,\text{max}} = 100\%$), and the compressor frequency is also increased to provide additional cooling for zone 2. In turn, this increased compressor frequency causes a disturbance in the air temperature in zone 1, which is rejected through CCC_1.

Fig. 3B-i shows the time varying reference of the compressor discharge temperature, which is computed from the compressor frequency according to (6a). Both controllers are tuned such that the compressor discharge temperature is allowed to deviate from its reference so that tracking other references and satisfying constraints may be prioritized. A maximum constraint is enforced on the discharge temperature during two periods in the simulations, where the small violations are permitted by constraint softening.

Comparing the performance of reconfigurable MPC to that of the collection of MPC controllers, negligible difference is observed in the overall transient behavior, except minor differences in command rates of outdoor fan (ODF) speed when the evaporator in zone 2 is shut off. This may be caused by the slightly more conservative terminal cost of the reconfigurable MPC method, due to the required block diagonal structure of $\hat{\mathcal{P}}^{\text{s}}$ in equation (15).

Next, we validate these results by performing an experiment that aims to reproduce the simulated conditions. Using the experimental facility, the reconfigurable MPC controls the two-zone commercial ME-VCS. Referring to Fig. 4, the vapor compression system is configured with setpoints $\text{Tr}_{1,\text{ref}} = 25°\text{C}$, $\text{Tr}_{2,\text{ref}} = 20°\text{C}$ and the boundary conditions are set to $\text{Q}_1 = \text{Q}_2 = 1600\ W$, and OAT = 35°C.

Qualitatively, the experimental results of Fig. 4 largely resemble the simulated results of Fig. 3, and differences are attributed to slightly different test conditions (*e.g.* 1800 W simulated loads vs. 1600 W experimental loads, different MPC constraints (*e.g.* faster rate limits on CF used in experiment) and mismatch between a linear simulation model and the true nonlinear dynamics of the real system. Despite these differences, we conclude that the simulations comparing reconfigurable MPC to a collection of controllers accurately reflect the dynamics of the experimental system.

The simulation and associated validation experiment in this section reset the actuator for the zone switched off to the origin in the linearized coordinates $u_2 = 0$, which is $\text{CCC}_2 = 65\%$ in engineering units. This strategy maintains the system dynamics near the operating point about which the linear model was obtained, and therefore enables fair comparison of controller performance without introducing strong nonlinearities from the physical system operated away from the linearization point. However, when an evaporator is to be turned off in the real system (due to low loads in the associated zone), the appropriate control action is to fully close the EEV in order to stop refrigerant flow. However, this method of operation emphasizes nonlinearities in the system dynamics, and understanding the robustness to this nonlinear effect is explored in the following experiments in which the EEV is fully closed when the associated zone is turned off.

V. Advanced Experimental Validation

In this section, the reconfigurable MPC is tested under more strenuous conditions. In Section V-A the configuration of the ME-VCS is changed while a plant output constraint is active. In Section V-B a supervisory state machine algorithm automatically reconfigures the closed-loop system.

A. Enforcing Constraints During Reconfiguration

This section describes an experiment where a step change to a setpoint is applied in order to induce a transient response where an output constraint becomes active. While the constraint is active, the ME-VCS is reconfigured to turn on a zone, and the output constraint remains enforced during the remainder of the transient.

Referring to Fig. 5, the vapor compression system is configured for single zone operation with a setpoint $\text{Tr}_{1,\text{ref}} = 25°\text{C}$ and the boundary conditions Q_1 = 2200 W, and OAT = 35°C. Initially zone 2 is off, and $\text{CCC}_2 = 0\%$ (engineering units, not linearized units as in the previous section) which equates to a fully closed EEV_2 and therefore no refrigerant flows through the evaporator. The initial load in zone 2 is 0 W, and the initial zone temperature is $Tr_2 = 29.5°\text{C}$ (Fig. 5B-iii).

At $t = 5$ min, the setpoint for zone 1 is lowered to $\text{Tr}_{1,\text{ref}} = 22°\text{C}$ (Fig. 5B-ii), and the controller increases the CF and saturates CCC_1 to reduce the temperature in that zone. As a result of the increased CF, the discharge temperature begins to increase until it reaches its constraint at $t = 8$ min (Fig. 5B-i). The CF commands subsequently selected by the MPC are modulated to maintain Td at or below its constraint.

After the Td constraint has been active for 2 minutes, zone 2 is switched on. CCC_2 is set to 75% and the MPC is reconfigured to enable control of this input. Simultaneously, an 1800 W load is applied to zone 2, and together with the 2200 W load in 1, it is a significant amount of heat with a restrictive (and active) constraint on Td.

From $t = 20$ to 35 minutes, Td largely follows the constraint until at about $t = 35$ min a constraint violation of about 2°C occurs (Fig. 5B-i), which is attributed to modeling errors. Additionally, the CCC_1 input is also saturated at its maximum value (Fig. 5A-i), making two constraints active during this transient. The Td constraint violation causes an immediate reduction in CF at $t = 35$ min, and Td is decreased accordingly, relieving the violation. Finally, both zones achieve their setpoints with zero steady state error at $t = 50$ min.

The oscillatory behavior of the CCC_2 command (Fig. 5A-iii) and associated response of Tr_2 (Fig. 5B-iii) is attributed

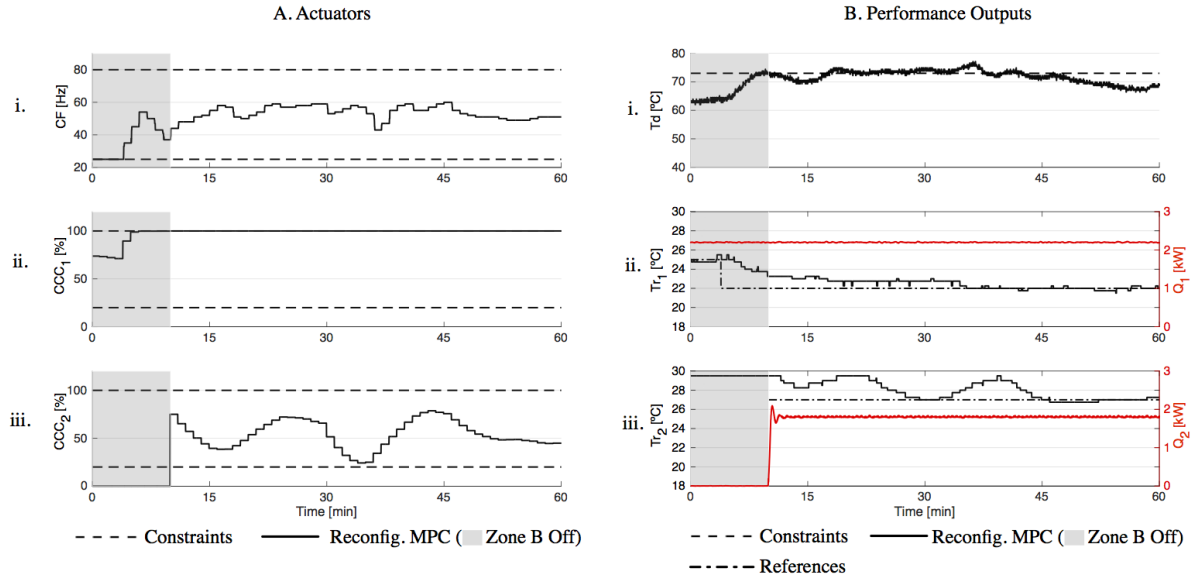

Fig. 5. Enforcing constraints during controller reconfiguration. With zone 2 turned off, the setpoint temperature in zone 1 is reduced, causing the compressor discharge temperature Td to constraint to become active. With this constraint active, zone 2 is turned on and a load step is applied, and the discharge temperature constraint is enforced throughout the transient.

to a combination of aggressive tuning of performance weights in the cost function, experimental operation at conditions different than the linearized model, and an interaction with a nonlinear resetting integrator. Further discussion of nonlinear integrators and their interaction with reconfigurable MPC is beyond the scope of the present work.

Despite the oscillatory behavior in zone 2, this experiment demonstrates that a plant output constraint can be enforced before and after system reconfiguration. Further, a reconfigurable MPC designed from a linear model when both zones are active can applied to a configuration with one zone switched off and still maintain setpoint tracking performance and constraint enforcement. The ability to reconfigure the MPC provides flexibility in application that is exploited in the next section to create a realistic control system (MPC under the direction of a supervisory state machine) that automatically turns zones on or off based on the per-zone loading conditions.

B. Automatic Reconfiguration

A production-ready control system for a multi-evaporator vapor compression system must turn zones on or off autonomously in order to regulate zone temperatures when the heat loads are lower than the minimum continuously-available cooling capacity. In the context of this work, this requires supervisory logic to automatically determine the system configuration $\varsigma(t)$. In this section, a state machine is designed to detect low heat load conditions and reconfigure the ME-VCS as conditions require.

Whereas Theorem III.4 shows the stability of the configuration-dependent controller (i.e., for a given configuration), stability of the overall switched system requires sufficient dwell time between changes in the configuration [24]. The objective of this experiment is to empirically demonstrate reference tracking and constraint enforcement of the reconfigurable MPC controlling a switching system where the dwell times for a particular configuration are determined by an autonomous supervisory state machine. The state machine logic considers the sign and magnitude of the zone temperature error signal and associated cooling command to determine when to switch a zone on or off. Specifically, if a zone is off and has become overheated by 1°C, then the state machine will turn that zone on. If a zone is on and either the zone has become overcooled by 2.5°C, or the cooling capacity command for that zone has been low enough for long enough, then the zone is turned off.

Regarding the latter condition, an integrator is used to determine the low actuator condition as follows: If CCC_i is less than 40%, then an integrator state $e_i(t)$ increases according to

$$e_i(t+1) = e_i(t) + (40 - \text{CCC}_i) \tag{30}$$

Once the integrator has reached a predetermined value, then condition (2) has been met and the zone is turned off. This predetermined value is chosen so that if CCC_i has been at its low constraint of 20% for about 5 minutes, then condition (2) becomes true. This test on the cooling capacity command will cause a zone to be turned off even if good setpoint tracking is achieved, but requires a low capacity command to do so, which is the intended behavior. The parameters used in the state machine have been determined heuristically. This state machine operates as a supervisory algorithm for the reconfigurable MPC, and coordinates operation such that actuator commands and integrators states are zeroed when reconfiguration occurs.

Using this state machine to automate the zone on/off signal $\varsigma(t)$, an experiment is conducted wherein the heat load in zone 2 is reduced. Referring to Fig. 6, the vapor compression system is brought into steady state operation with setpoints $\text{Tr}_{1,\text{ref}} = 21°\text{C}$, $\text{Tr}_{2,\text{ref}} = 25°\text{C}$ and the boundary conditions are set to $\text{Q}_1 = \text{Q}_2 = 1800\ W$, and OAT = 35°C. At this

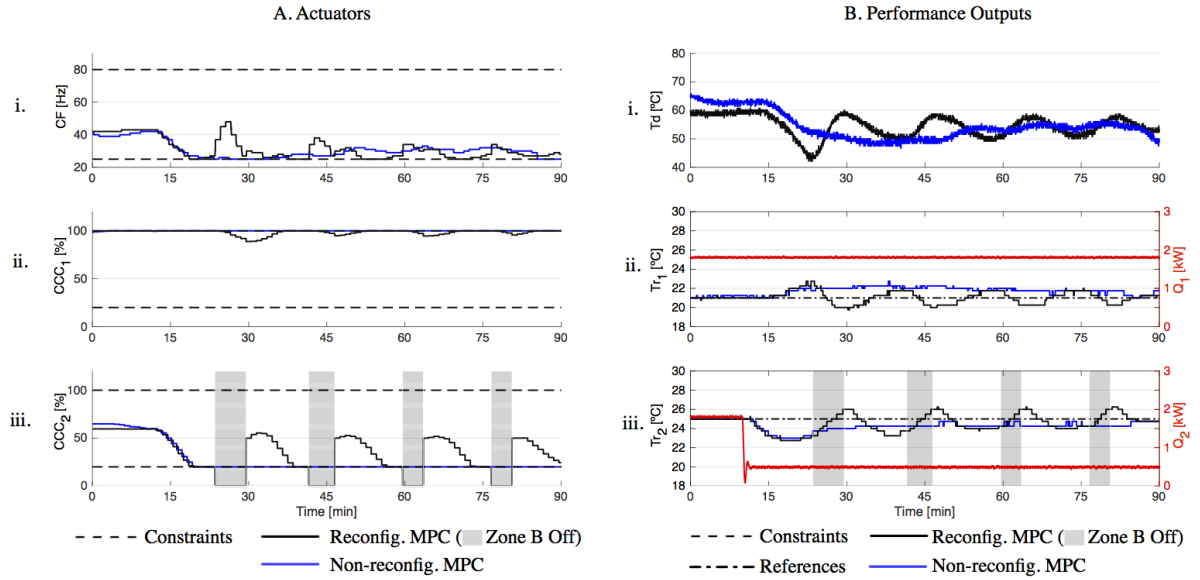

Fig. 6. Automatic reconfiguration during low load conditions. An experiment is shown in which the applied thermal load is lower than the minimum capacity continuously available from the zone evaporator and therefore requires the machine to begin "low load cycling." The reconfigurable MPC is shown to drive the two zone temperatures to their respective setpoints on average while a non-reconfigurable controller results in steady state errors.

initial condition, both zone loads are met in steady state with a compressor frequency of CF = 40 Hz, and cooling capacity commands of CCC_1 = 100% and CCC_2 = 60%.

At $t = 10$ min, the heat load in zone 2 is decreased to 500 W, which is a load that is about equal to the cooling provided when operated at $CCC_{2,\min}$ = 20%. As a result of the load step, the temperature in zone 2 is reduced, and the MPC decreases the associated actuator command to its minimum value in an attempt to raise the zone temperature back to the setpoint.

After about 10 minutes, the integrator in the supervisory state machine has reached its predetermined value, and ς_2 is set to 0, triggering reconfiguration of the controller. Zone 2 is automatically switched off, and the CCC_2 command is set to 0 (Fig. 6A-iii, black), which closes the associated EEV. The zone temperature subsequently increases under the influence of the 500 W load until it becomes overheated by 1°C (Fig. 6B-iii, black), at which point the state machine sets ς_2 to 1 and the controller is again reconfigured to turn zone 2 back on. This pattern is repeated under automatic control, establishing a cyclic response.

Note that the coupling inherent in the vapor compression system induces a periodic disturbance in zone 1 (Fig. 6B-ii, black) as zone 2 is switched on and off, which can only be partially rejected since the associated actuator CCC_1 is saturated at its maximum value for large periods of the disturbance cycle (Fig. 6A-ii, black). Despite the large imbalance in loads between the two zones, both zone temperatures cycle around their respective setpoints, and when averaged over multiple periods, both zones are shown to achieve their setpoints. The experiment demonstrates that the reconfigurable MPC can operate in combination with supervisory logic determining the on/off conditions.

Fig. 6 also shows the same experiment for the case where the controller is not permitted to reconfigure. This non-reconfigurable MPC is shown in blue for the same test conditions. Since the controller cannot turn zone 2 off, CCC_2 is driven to its lower limit (Fig. 6A-iii, blue) while CCC_1 remains saturated at its upper limit (Fig. 6A-ii, blue). The corresponding temperatures for these zones settle to a nonzero steady state error (about 1°C overheated in zone 1 (Fig. 6B-ii, blue), and about 1°C overcooled in zone 2 (Fig. 6B-iii, blue)). Note that since both zone temperature tracking errors are equally penalized in the cost function, the MPC controller selects compressor frequency commands that equally distribute the zone tracking errors despite both zone capacity commands being saturated. Whereas the non-reconfigurable approach results in persistent steady state errors, the reconfigurable MPC permits low-load cycling to meet the zone setpoints on average.

In summary, experiments presented in this section demonstrate that reconfigurable MPC drives performance outputs to their references, rejects disturbances and enforces constraints before and after reconfiguration. Further, despite similar transient performance, reconfigurable MPC is orders-of-magnitude more efficient in memory storage requirements and tuning effort than traditional approaches. Finally, reconfiguration is automated with a supervisory state machine, a required feature for wide-scale deployment.

VI. Conclusions

Reconfigurable MPC is presented for a multi-evaporator vapor compression system where indoor units are permitted to turn on or off. Whereas a traditional MPC approach requires separate controllers for each configuration that must be designed and tuned and where parameters that define each controller must be stored on the embedded platform, reconfigurable MPC uses a single controller formulation and online updates to the parameterized cost. The approach is compared to a collection of independently-designed model predictive controllers and validated in experiments.

Daniel J. Burns Daniel Burns received the M.S. and Ph.D. degrees in mechanical engineering from the Massachusetts Institute of Technology, Cambridge, in 2006 and 2010, respectively. Since 2010, he has been with Mitsubishi Electric Research Laboratories (MERL), Cambridge, MA, where he is currently a Principal Research Scientist. At MERL, Dr. Burns develops and prototypes advanced control methods for vapor compression systems. Before joining MERL, he worked on flight instrumentation and control at the Commercial Aviation Systems division of Honeywell, Inc. and NASA's Goddard Space Flight Center. His research interests include multi-physical modeling and control of mechatronic and thermodynamic systems, instrumentation and experimentation, and applied predictive and adaptive control.

Claus Danielson Claus Danielson received his PhD in 2014 from the Model Predictive Control Laboratory at the University of California, Berkeley. He is currently a Research Scientist at Mitsubishi Electric Research Laboratories in Cambridge, MA. His research interests are in predictive and constrained control. His specialty is developing methods for exploiting structure in large-scale or complex control and optimization problems. He has applied his research to a variety of fields include energy storage networks, heating ventilation and air conditioning, adaptive optics, spacecraft guidance and control, atomic force microscopy, autonomous vehicles, cancer treatment, and robotics.

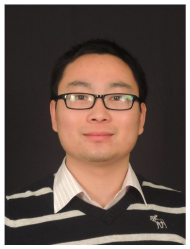

Junqiang Zhou Junqiang Zhou received the M.S. and Ph.D. degrees in Mechanical Engineering from The Ohio State University in 2013 and 2015, respectively. During May-August 2015, he was a research intern at Mitsubishi Electric Research Laboratory, Cambridge, MA. Since 2016, he has been with GE Global Research Center, Niskayuna, NY. His research interests span the field of dynamical system and control theory, model predictive control with emphasis on tracking and output regulation and applications to automotive systems and thermal-fluid energy systems. His current projects include control and optimization of combined-cycle power plant and wind turbines.

Stefano Di Cairano (M'08) Stefano Di Cairano received the Master (Laurea), and the PhD in Information Engineering in '04 and '08, respectively, from the University of Siena, Italy. During '08–'11, he was with Powertrain Control R&A, Ford Research and Adv. Engineering, Dearborn, MI. Since 2011, he is with Mitsubishi Electric Research Laboratories, Cambridge, MA, where he is the Senior Team Leader for Optimization-based Control, and a Senior Principal Researcher in Mechatronics. His research is on optimization-based control strategies for complex mechatronic systems, in automotive, factory automation, transportation and aerospace. His research interests include model predictive control, constrained control, networked control systems, hybrid systems, optimization.

Dr. Di Cairano has authored/co-authored more than 100 peer reviewed papers in journals and conference proceedings, and 25 patents/patent applications. He was the Chair of the IEEE CSS Technical Committee on Automotive Controls, is the Chair of IEEE Standing Committee on Standards, and an Associate Editor of the IEEE Trans. Control Systems Technology.

REFERENCES

[1] X. D. He, S. Liu, H. H. Asada, and H. Itoh, "Multivariable control of vapor compression systems," *HVAC&R Research*, vol. 4, no. 3, pp. 205–230, July 1998.

[2] N. Jain, D. J. Burns, S. Di Cairano, C. R. Laughman, and S. A. Bortoff, "Model predictive control of vapor compression systems," in *15th International Refrigeration and Air Conditioning Conference at Purdue, July, 2014*, 2014.

[3] M. Wallace, B. Das, P. Mhaskar, J. House, and T. Salsbury, "Offset-free model predictive control of a vapor compression cycle," *Journal of Process Control*, vol. 22, no. 7, pp. 1374–1386, August 2012.

[4] M. Wallace, P. Mhaskar, J. House, and T. I. Salsbury, "Offset-free model predictive control of a heat pump," *Industrial & Engineering Chemistry Research*, vol. 54, no. 3, pp. 994–1005, 2015.

[5] J. Koeln and A. Alleyne, "Scalable model predictive control for multi-evaporator vapor compression systems," in *American Control Conference (ACC), 2014*, June 2014, pp. 392–397.

[6] M. S. Elliott and B. P. Rasmussen, "Decentralized model predictive control of a multi-evaporator air conditioning system," *Control Engineering Practice*, vol. 21, no. 12, SI, pp. 1665–1677, December 2013.

[7] J. P. Koeln and A. G. Alleyne, "Decentralized Controller Analysis and Design for Multi-Evaporator Vapor Compression Systems," in *American Control Conference (ACC), 2013*, 2013, pp. 437–442.

[8] J. Stoustrup, "Plug & play control: Control technology towards new challenges," *European Journal of Control*, vol. 15, no. 3, pp. 311–330, 2009.

[9] J. Bendtsen, K. Trangbaek, and J. Stoustrup, "Plug-and-play control: Modifying control systems online," *IEEE Transactions on Control Systems Technology*, vol. 21, no. 1, pp. 79–93, 2013.

[10] S. Riverso, M. Farina, and G. Ferrari-Trecate, "Plug-and-play model predictive control based on robust control invariant sets," *Automatica*, vol. 50, no. 8, pp. 2179–2186, 2014.

[11] M. N. Zeilinger, Y. Pu, S. Riverso, G. Ferrari-Trecate, and C. N. Jones, "Plug and play distributed model predictive control based on distributed invariance and optimization," in *52nd Annual Conference on Decision and Control (CDC)*. IEEE, 2013, pp. 5770–5776.

[12] S. Riverso, F. Boem, G. Ferrari-Trecate, and T. Parisini, "Fault diagnosis and control-reconfiguration in large-scale systems: a plug-and-play approach," in *2014 IEEE 53rd Annual Conference on Decision and Control (CDC)*. IEEE, 2014, pp. 4977–4982.

[13] S. Di Cairano and A. Bemporad, "Model predictive control tuning by controller matching," vol. 55, no. 1, pp. 185–190, 2010.

[14] S. Di Cairano, "Model adjustable predictive control with stability guarantees," in *American Control Conference (ACC), 2015*, July 2015, pp. 226–231.

[15] D. Burns and S. Bortoff, "Cooling Capacity Control for Multi-Evaporator Vapor Compression Systems," in *16th International Refrigeration and Air Conditioning Conference at Purdue*, 2016.

[16] N. Jain, J. P. Koeln, S. Sundaram, and A. G. Alleyne, "Partially decentralized control of large-scale variable-refrigerant-flow systems in buildings," *Journal of Process Control*, vol. 24, no. 6, pp. 798–819, 2014.

[17] D. Burns and C. Laughman, "Extremum seeking control for energy optimization of vapor compression systems," in *14th International Refrigeration and Air Conditioning Conference at Purdue*, July 2012.

[18] G. Pannocchia and J. B. Rawlings, "Disturbance models for offset-free model-predictive control," *AIChE journal*, vol. 49, no. 2, pp. 426–437, 2003.

[19] U. Maeder, F. Borrelli, and M. Morari, "Linear offset-free model predictive control," *Automatica*, vol. 45, no. 10, pp. 2214–2222, 2009.

[20] S. Di Cairano, J. Doering, I. Kolmanovsky, and D. Hrovat, "Model predictive control of engine speed during vehicle deceleration," *IEEE Transactions on Control Systems Technology*, vol. 11, no. 4, 2012.

[21] M. Lazar, "Model predictive control of hybrid systems: Stability and robustness," 2006.

[22] D. Liberzon, *Switching in systems and control*. Springer Science & Business Media, 2003.

[23] C. A. Floudas, *Nonlinear and Mixed-Integer Optimization*. Oxford University Press, 1995.

[24] L. Bridgeman, C. Danielson, and S. Di Cairano, "Stability and feasibility of MPC for switched linear systems with dwell-time constraints," in *American Control Conference (ACC)*, 2016.

[25] S. Di Cairano, M. Brand, and S. A. Bortoff, "Projection-free parallel quadratic programming for linear model predictive control," *International Journal of Control*, vol. 86, no. 8, pp. 1367–1385, 2013.